

# Semantic Structure-Aware Generative Attacks for Enhanced Adversarial Transferability

Jongoh Jeong, Hunmin Yang, Jaeseok Jeong, Kuk-Jin Yoon  
Visual Intelligence Lab., KAIST  
{jeong2, hmyang, jason.jeong, kjyoon}@kaist.ac.kr

## Abstract

Generative adversarial attacks train a perturbation generator on a white-box surrogate model and subsequently apply the crafted perturbations to unseen black-box victim models. In contrast to iterative attacks, these methods deliver superior inference-time efficiency, scalability, and transferability; however, up until now, existing studies have not fully exploited the representational capacity of generative models to preserve and harness semantic information. Specifically, the intermediate activations of the generator encode rich semantic features—object boundaries and coarse shapes—that remain under-exploited, thereby limiting the alignment of perturbations with object-salient regions which are critical for adversarial transferability. To remedy this, we introduce a semantic structure-aware attack framework based on the Mean Teacher, which serves as a temporally smoothed feature reference. With this smoothed reference, we further direct semantic consistency between the early-layer activations in the student and those of the semantically rich teacher by feature distillation. By anchoring perturbation synthesis to the semantically salient early intermediate blocks within the generator based on empirical findings, our method guides progressive adversarial perturbation on regions that substantially enhance adversarial transferability. We conduct extensive experiments over diverse models, domains and tasks to demonstrate consistent improvements relative to state-of-the-art generative attacks, comprehensively evaluated using conventional metrics and our newly proposed Accidental Correction Rate (ACR). Code will be made publicly available upon publication.

## 1 Introduction

Deep neural networks have driven transformative advances across computer vision, natural language processing, and medical diagnosis. Their capacity to learn rich, hierarchical feature representations has enabled breakthroughs in tasks ranging from fine-grained image classification to complex sequence generation. Yet these models remain alarmingly fragile: even small, human-imperceptible perturbations—known as adversarial examples (AEs) [58]—can provoke confident misclassification, underscoring the need to safeguard real-world deployments against malicious exploits. The threat is further intensified in black-box scenarios, where attackers have no access to a model’s architecture or parameters. In such scenarios, transferable ad-

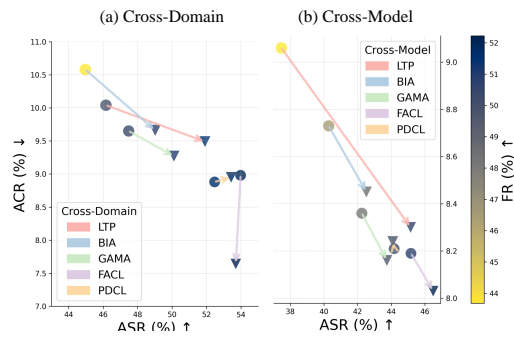


Figure 1: Our semantic structure-aware attack effectively exploits the intermediate block features to craft adversarial examples for enhanced transferability (▼) from the baselines (●) across domains (a) and models (b).

versarial attacks craft perturbations on a surrogate network and deploy the same perturbation against unknown targets. This capability empowers adversaries to compromise multiple real-world systems, such as autonomous vehicles, biometric scanners, and diagnostic tools, with a single perturbation strategy, posing severe risks to safety-critical applications.

Early white-box iterative attacks, such as FGSM [85] and its iterative variants [15, 76, 17], exploit gradient information directly but inherently require full model access. To evaluate real-world attack robustness, transfer-based (black-box) attacks emerged, leveraging the phenomenon that adversarial perturbations crafted on one model often fool others. While iterative gradient-based methods [43, 9, 85], whether operating in white-box or query-based modes, can yield moderately transferable adversarial examples, they incur intensive costs due to per-sample optimization steps, resulting in prohibitive computation time and slow inference. Such bottleneck prohibits their use in time-sensitive scenarios and limits scalable and practically deployable attacks.

To overcome this, generative transfer attacks [74, 68, 2, 3, 51, 50, 29, 86, 1, 81–83, 48] aim to train a dedicated perturbation generator against a surrogate, enabling fast inference and high transfer rates without per-example optimization. Generative attacks address these limitations by training a feed-forward generator to produce perturbations in one pass. Once trained, this generator yields adversarial noise with a single forward inference, offering orders-of-magnitude improvements in speed, seamless scalability to large datasets, and strong transferability. However, existing generative frameworks predominantly treat the generator as a black box, optimizing only end-to-end metrics while overlooking how semantic information, such as object edges and coarse shapes, is represented and potentially degraded within its intermediate layers. As a result, crafted perturbations may be dispersed onto irrelevant background regions, diluting both stealth and cross-domain/model efficacy.

This naturally raises two fundamental questions: (1) *At which stage do semantic cues deteriorate under adversarial synthesis?* and (2) *Which generator intermediate blocks most influence transferability?* To respond to these questions, we partition the generator’s feature maps into early, mid, and late blocks and show empirically that early blocks uniquely preserve the benign input’s semantic integrity (*i.e.*, object contours, shape priors) while later blocks progressively erode these cues due to added perturbations.

To address these questions, we conduct a systematic analysis into the progression of adversarial perturbation generation in the generator’s feature level by partitioning its intermediate activations into early, mid, and late blocks. Our empirical study reveals that early intermediate blocks retain the most semantic structure of the benign input, *i.e.*, object boundaries and coarse shapes, while later blocks progressively dilute these cues as perturbations accumulate. Guided by this insight, we propose a semantic structure-aware generative framework, as shown in Fig. 2, that (1) integrates a Mean Teacher paradigm to produce temporally smoothed reference features via exponential moving average (EMA) of student weights, and (2) enforces a feature distillation loss on the generator’s early-block activations, anchoring them to the semantically rich teacher features. By grounding perturbation synthesis in these early stages, our method further encourages the generator to focus perturbations on object-centric regions, further enhancing the transferability in multiple cross-settings as shown in Fig. 1. Finally, we identify shortcomings in the evaluation protocols adopted by previous works, and introduce a novel complementary metric, Accidental Correction Rate (ACR), to capture inadvertently corrected predictions, thereby providing a more comprehensive assessment of attack efficacy. We summarize our main contributions as follows:

- **Empirical analysis of generator features.** By dividing the generator’s layers into early, mid, and late blocks, we find that the early blocks consistently retain object contours and overall shape, whereas later blocks progressively erode these semantic cues as adversarial perturbations accumulate.
- **Semantic structure-aware generative framework.** We introduce a Mean Teacher-based attack in which an EMA-updated teacher provides noise-smoothed reference features, and a feature distillation loss aligns the student’s early-block activations to these semantically rich scaffolds of the teacher activations, thereby focusing perturbations on object-centric regions.
- **Comprehensive evaluation with a novel metric.** We identify shortcomings in existing protocols and propose the Accidental Correction Rate (ACR) to capture inadvertently corrected predictions. By evaluating across multiple models and domains using ACR alongside three conventional metrics (ASR, FR, Accuracy), we demonstrate consistent gains over state-of-the-art generative attacks as an add-on approach.

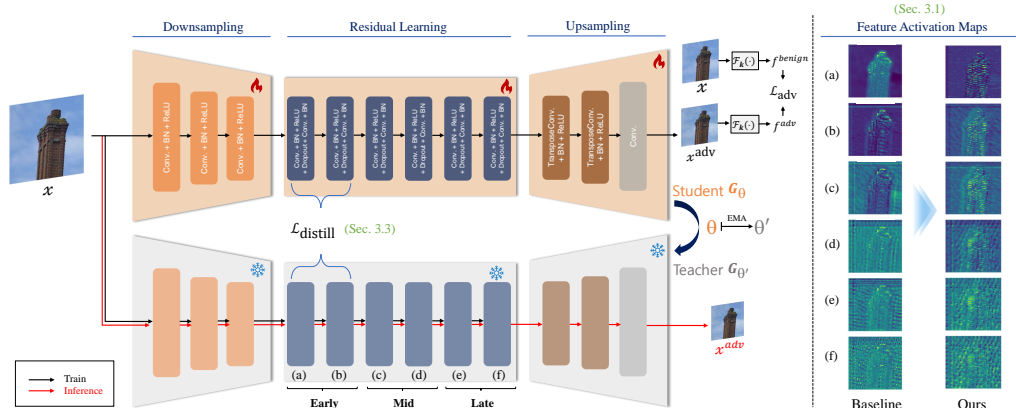


Figure 2: **Overview of our proposed framework.** Given a clean input image, a generative attack network produces an adversarial output under the supervision of a Mean Teacher structure. The student and teacher branches of the generator share architecture, with the teacher updated via exponential moving average (EMA) of the student. Semantic consistency is enforced by aligning their intermediate features, while feature distillation is selectively applied to early blocks to preserve structural information from the benign input. The adversarial example is then evaluated against a frozen surrogate model to compute the fooling objective. This joint design promotes semantic alignment—combining consistency and integrity—which enhances adversarial transferability across diverse target models.

## 2 Related Work

### 2.1 Transfer-based Adversarial Attacks

Transfer-based attacks exploit the empirical finding that adversarial perturbations crafted on one model often remain effective against others, even when architectures or training data differ. Early methods relied on iterative gradient-based strategies—momentum-integrated attacks (DI [77], TI [16]), input-diversity techniques (SI [39], Admix [71]), and strong baselines such as BIM [34], PGD [43], and C&W [9]. These approaches enhance transferability via gradient smoothing, input transformations, and ensemble gradients, but incur heavy per-example optimization costs and often struggle against architectures that diverge significantly from the surrogate.

More recent work has introduced generative frameworks that train feed-forward generators to synthesize perturbations in a single pass. GAP [51], CDA [50], and LTP [29] demonstrated orders-of-magnitude speedups with comparable transfer rates. Subsequent advances—BIA [86], GAMA [1], FACL-Attack [81], PDCL-Attack [83], and NAT [48]—have further improved robustness by integrating logit or mid-level layer feature divergence, frequency-domain constraints, text prompt-driven, and neuron-targeted losses. **Our distinctions.** Rather than focusing solely on end-to-end optimization or domain-level constraints, we analyze the generator’s intermediate feature hierarchy and preserve semantic fidelity in its early blocks to steer perturbations onto object-centric regions, thereby enhancing cross-model transfer effectiveness.

### 2.2 Generative Model-based Attacks

Generative attacks recast adversarial synthesis as a learning problem, training an image-to-image network (e.g. GAN or encoder–decoder) to produce perturbations in one pass. GAP [51] pioneered a framework in which the generator outputs adversarial noise that is then added to the input. CDA [70] extends this by training a transformation network that directly outputs adversarial examples. Subsequent works incorporate perceptual losses based on surrogate logits [29] and mid-level surrogate features [86, 48]. Building on the feature-similarity loss of Zhang et al. [86], more recent approaches leverage vision–language foundation models such as CLIP [52] [1, 83] and apply frequency-domain manipulations to surrogate features [82], further boosting transferability. **Our distinctions.** While prior frameworks prioritize perturbation realism or frequency characteristics, we explicitly target the generator’s internal semantics by combining Mean Teacher-based smoothing with feature distillation

on early blocks, preserving object contours and textures and concentrating adversarial perturbations in the most transferable regions.

### 2.3 Self-Knowledge Distillation

Self-knowledge distillation (Self-KD) aims to train a model to refine its own representations without an external teacher. Pioneering works in this field, Born-Again Networks [19] and Deep Mutual Learning [87], demonstrated that iterative self- and peer-distillation can improve generalization and robustness. Recent works [38, 84] incorporate self-kd by aligning logits or intermediate features within its own network, or progressively updating the network [30]. In this paradigm of using a student-teacher framework, the Mean Teacher framework [62], originally developed for semi-supervised learning, aims to maintain a teacher as the exponential moving average of the student’s weights, implicitly enforcing temporal consistency in predictions or feature maps. This EMA-based smoothing has been shown to reduce overfitting, stabilize training, and enhance domain invariance—properties that are directly relevant to generating perturbations that transfer across black-box models. **Our distinctions.** Departing from classification-centric distillation, we integrate the Mean Teacher paradigm into a generative attack pipeline, using EMA to smooth intermediate features and applying hinge-based feature distillation on early blocks to preserve semantic integrity critical for cross-setting transferability.

## 3 Proposed Method

### 3.1 Problem Formulation

Our framework for generative model-based untargeted transfer attacks comprises an adversarial perturbation generator  $\mathcal{G}_\theta(\cdot)$ , producing unconstrained adversarial examples  $x^{adv}$  from benign inputs  $x$ , which are then projected via a perturbation projector  $\mathcal{P}(\cdot)$  to satisfy  $\|\mathcal{P}(x^{adv}) - x\|_\infty \leq \epsilon$ . To train  $\mathcal{G}_\theta(\cdot)$  in a label-free manner in the untargeted attack, we employ a white-box surrogate model to provide an adversarial supervisory signal for generator updates via back-propagation. The adversarial loss uses mid-layer surrogate features  $\mathcal{F}_k(\cdot)$ , which contain model-shared characteristics that are crucial for adversarial transferability.

### 3.2 Motivation

Our motivation draws from an empirical observation of how perturbations evolve through the residual blocks within the generator after training (see Fig. 3). Given the ResNet-based generator architecture by previous works [50, 29, 86, 1, 82, 83], we visualized the output activation maps from the *intermediate* layers, as *most of the noise is added in the residual intermediate blocks* as pointed out by [86].

While early intermediate blocks consistently retain the object’s coarse structure, mid and late blocks progressively erode these semantic cues, dispersing perturbations indiscriminately. Moreover, state-of-the-art methods that better preserve early-stage semantics tend to yield higher black-box transferability across models, domains, and tasks. This suggests that maintaining the generator’s internal semantic structure in its early layers is crucial to transferability: by anchoring the generated perturbations to these semantically consistent features, subsequent blocks naturally learn to concentrate adversarial perturbation on object-salient regions. Consequently, we seek to explicitly preserve early-block semantics so that later-stage perturbations focus more effectively on object-salient regions that can generalize across various models.

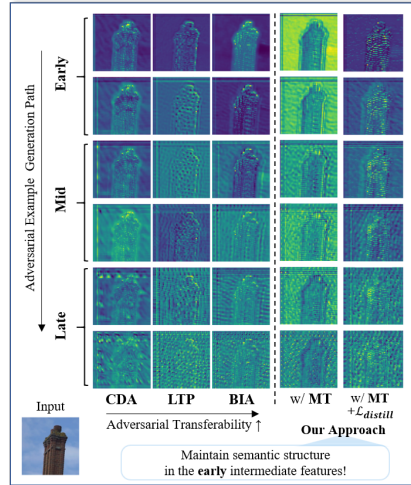


Figure 3: Visualization of activation maps from the residual intermediate blocks within the trained generator. Note that the semantic structure is mostly retained in the early stage compared to mid and late stages.



---

**Algorithm 1:** Pseudo-code for Semantic Structure-Aware Attack

---

**Data:** Training dataset  $\mathcal{D}_{train}$ **Input :** Generator  $\mathcal{G}_\theta(\cdot)$ , a frozen surrogate model  $\mathcal{F}_k(\cdot)$ , projector  $\mathcal{P}(\cdot)$ , perturbation budget  $\epsilon$ **Output :** optimized teacher perturbation generator  $\mathcal{G}_{\theta'}(\cdot)$ 

```
1 Randomly initialize student  $\mathcal{G}_\theta(\cdot)$ , and teacher  $\mathcal{G}_{\theta'}(\cdot)$  with student weights  $\theta$ 
2 repeat
3   Randomly sample a mini-batch  $x_i$  from  $\mathcal{D}_{train}$ 
4   Acquire student generator features:  $\mathbf{g}_{i,s} \leftarrow \mathcal{G}_\theta^{\text{enc}}(x_i)$ 
5   Acquire teacher generator features:  $\mathbf{g}_{i,t} \leftarrow \mathcal{G}_{\theta'}^{\text{enc}}(x_i)$ 
6   Generate unbounded adversarial examples:  $x_i^{\text{adv}} \leftarrow \mathcal{G}_\theta^{\text{dec}}(\mathbf{g}_{i,s})$ 
7   Project  $x_i^{\text{adv}}$  using the projector  $\mathcal{P}$  within the perturbation budget:  $\|\mathcal{P}(x_i^{\text{adv}}) - x_i\|_\infty \leq \epsilon$ 
8   Forward pass  $x_i$  and  $x_i^{\text{adv}}$  through surrogate to acquire  $f_i^{\text{benign}}, f_i^{\text{adv}}$ 
9   Compute loss using  $f_i^{\text{benign}}, f_i^{\text{adv}}, \mathbf{g}_{i,s}, \mathbf{g}_{i,t}$ :  $\mathcal{L} = \mathcal{L}_{\text{adv}} + \lambda_{\text{distill}} \cdot \mathcal{L}_{\text{distill}}$  // Eqs. 2, 4
10
11   Update student generator parameters via backpropagation
12   EMA update teacher weights with student weights:  $\theta \mapsto \theta'$ 
13 until  $\mathcal{G}_\theta(\cdot)$  converges
```

---

### 3.3 Proposed Framework

Our semantic structure-aware attack, as described in Alg. 1, augments a standard generative adversarial attack with two key components: a Mean Teacher-based feature smoothing and a self-feature distillation loss that enforces semantic consistency in early generator layers. We base our approach on the baseline work [86] because all the subsequent works [1, 82, 83] base their losses on the feature similarity-based adversarial loss suggested by [86], thus it is adequate to serve as a solid baseline.

**Role of Mean Teacher.** The Mean Teacher (MT) framework [62, 13, 37, 88, 7, 14] has consistently demonstrated robustness in tasks characterized by significant domain shifts between training and testing. Its core mechanism of updating the teacher’s parameters with EMA of the student’s parameters provides a form of temporal ensembling that naturally suppresses instance-specific noise. Intuitively, this EMA update smooths out high-frequency perturbation artifacts, enriching the semantic consistency and stability of the teacher’s intermediate feature maps. As a result, these smoothed features serve as a reliable reference for the student, helping to preserve object contours and shapes throughout adversarial synthesis. To integrate MT, we maintain two generators: a *student*  $G_\theta$  that is trained via gradient descent, and a *teacher*  $G_{\theta'}$  whose parameters are updated by Eq. 1. We set these mean teacher features as a reference for our distillation component.

$$\theta' \leftarrow \eta \theta + (1 - \eta) \theta, \quad \eta \in [0, 1]. \quad (1)$$

**Self-feature distillation.** Object-salient intermediate representations have been shown to be critical for adversarial transfer in black-box settings [73, 5, 31, 86], and recent work has explored manipulating input or surrogate-level features to this end [27, 36, 48]. In our generative framework, however, a naïve generator progressively loses semantic integrity in its intermediate layers (Fig. 2), scattering perturbations away from object-salient regions. To preserve these crucial object cues, we introduce a self-distillation mechanism grounded in the Mean Teacher paradigm [62, 21, 10, 35].

Concretely, we treat the EMA-updated teacher as a source of temporally smoothed, semantically rich features. At each training iteration, we extract early-block activations from both student and teacher and enforce semantic consistency via a hinge-based distillation loss as follows:

$$\mathcal{L}_{\text{distill}} = \sum_{\ell=1}^{L_{\text{early}}} \mathcal{W}_{\text{distill}} \max(0, \tau - \cos(\mathbf{g}_s^{(\ell)}, \mathbf{g}_t^{(\ell)})), \quad (2)$$

where  $\cos(\cdot, \cdot)$  is cosine similarity and  $\tau$  a similarity threshold. This loss anchors the student’s edges and shape priors to the teacher’s smoothed semantics, ensuring that subsequent perturbations concentrate on object-centric regions.  $\mathcal{W}_{\text{distill}} \in \mathbb{R}^{|L|}$  denotes the softmax output of a learnable parameter for intermediate block-wise loss weighting. When combined with the adversarial objective, this self-feature distillation yields perturbations that are both highly transferable and tightly aligned

with the image’s core structure. For fair comparisons with the state-of-the-art methods, we adopt the adversarial loss in the surrogate feature space as practiced in the baseline [86].

$$\mathcal{L}_{\text{adv}} = \cos(\mathcal{F}_k(x), \mathcal{F}_k(x^{\text{adv}})) \quad (3)$$

**Final loss objective.** Putting the proposed and baseline losses together on MT framework, we formulate the final loss objective with  $\lambda_{\text{distill}}$  as a weight term for  $\mathcal{L}_{\text{distill}}$ , as follows:

$$\mathcal{L} = \mathcal{L}_{\text{adv}} + \lambda_{\text{distill}} \cdot \mathcal{L}_{\text{distill}}. \quad (4)$$

## 4 Experiments

### 4.1 Implementation details

Throughout the experiments, we train the perturbation generator with  $\epsilon = 10$  using data from ImageNet-1K [55] containing 1.2 M natural images of  $224 \times 224 \times 3$  resolution, following [51, 50, 29, 86, 1, 81–83]. We also use the mid-level layer feature at  $k = 16$  (Maxpooling.3) of VGG-16 surrogate for our baseline [86]. We set  $\lambda_{\text{distill}} = 0.7$  throughout our experiments for stable generator training at the feature level, and the EMA update parameter  $\eta = 0.999$  following [62]. We selected  $L_{\text{early}} = \{1, 2\}$  for distilling the first and second intermediate residual blocks within the generator. We compare our attacks against the state-of-the-art baselines that rely on the same ResNet-based generator to craft adversarial examples, *i.e.*, CDA [50], LTP [29], BIA [86], GAMA [1], FACL-Attack [81, 82], and PDCL-Attack [83].

### 4.2 Evaluation settings

We evaluate adversarial transfer under two black-box protocols. In the cross-model setting, perturbations are crafted on surrogate models trained with the same data distribution (ImageNet-1K [55]) and then tested on unseen target architectures. In the cross-domain/task settings, adversarial examples are to generalize across domain/task shifts without access to any target-distribution samples.

**Victim models.** For *cross-model* evaluation, we employ ImageNet-1K ( $224 \times 224$  resolution, 1,000 classes) pre-trained classification models of various architectures with their publicly available model weights. We source the pre-trained models from TorchVision [46] and Timm [72] libraries. Compared to previous approaches [29, 82, 83] demonstrating cross-model architecture transferability, we expand the evaluation to a wider scope of target model architectures for enhanced architecture-agnostic transferability. We test our attack against a total of 22 different model architectures (12 CNN-based [24, 26, 59, 53, 61, 28, 60, 69], 6 ViT-based [66, 41, 64, 4, 6], 2 Mixers [63, 65], and 2 Vision Mamba-based [89, 23]) for cross-model evaluations as in Table 1.

For *cross-domain* evaluation, we validate our attack against three different models (*i.e.*, ResNet50 [24], SE-Net and SE-ResNet101 [25]) pre-trained on fine-grained datasets, CUB-200-2011 [67] (200 classes), Stanford Cars [33] (196 classes), FGVC Aircraft [45] (100 classes), of  $448 \times 448$  resolution. We detail statistics and descriptions in the Appendix. For *cross-task*, we select a CNN-based and a ViT-based model for each task of semantic segmentation (SS) and object detection (OD), whose pre-trained weights are openly accessible as with the ImageNet-1K pre-trained weights. Specifically, we test against DeepLabV3+ [11] and SegFormer [78] for SS and Faster R-CNN [20] on detectron2 and DETR [8] for OD. We validate on Cityscapes [12] and COCO’17 [40] for SS and OD tasks, respectively.

**Against robust models.** We also test our attack against robust models, *i.e.*, adversarially trained Inception-V3 [34], ViT [18] and ConvNeXt [57] models, and robust input processing methods such as JPEG (75%) [22], bit reduction (BDR; 4-bit) [80] and randomization (R&P) [75] in Table 8.

**Evaluation metrics.** While developing an effective attack mechanism is crucial, it must be validated by fair and comprehensive evaluations. Current evaluation protocols adopted by prior works [51, 50, 29, 86, 1, 82, 83, 48] exhibit three key limitations. First, most studies report only a single primary metric (either one of Attack Success Rate (ASR), Fooling Rate (FR), or Top-1 Accuracy (%)), offering only a one-dimensional view of attack robustness and neglecting other aspects such as unintended corrections in predictions. Second, datasets and sample sizes are often selected arbitrarily or limited

Table 1: **Quantitative cross-model transferability results.** We report the average improvement margins of our method added to each baseline, averaged over three models for each domain. We report the improvements ( $\Delta\%$ ) with ours relative to each baseline. Better averaged results are marked in **boldface**.

Cross-model		CNN										Transformer										Mixer		Mamba		Avg.
Method	Metric	Res50	Res152	Dense121	Dense169	IncV3	RegNetY	Mnas	SqueezeV2	EfficientV2	HRNet	ConvNeXt	ResNeXt	ViT-B	ViT-L	Swin-B	DeiT-B	BeiT-B	EfficientViT	MLP-B	Conv-B	Vim	Mamba	Vision		
Benign	Acc. $\downarrow$	74.60	77.33	74.22	75.74	76.19	76.79	66.50	61.96	67.91	63.65	82.12	76.64	77.24	77.56	79.78	82.27	83.95	69.97	72.26	78.04	77.89	82.72	74.28		
CDA	Acc. ( $\Delta\%$ ) $\downarrow$	-15.93	-8.39	-12.93	-12.70	-8.41	-11.21	-5.09	-6.48	-10.17	-12.59	-35.91	-19.74	-0.59	-0.79	-21.93	-5.83	-2.23	-4.05	-3.48	-19.18	-30.11	-0.21	-11.27		
w/ Ours	FR ( $\Delta\%$ ) $\uparrow$	+17.39	+9.29	+14.24	+14.30	+8.96	+11.91	+5.87	+7.86	+11.49	+15.54	+38.92	+21.57	+1.06	+1.72	+24.10	+6.90	+2.74	+5.15	+4.22	+20.77	+33.98	+0.30	+12.63		
	ACR ( $\Delta\%$ ) $\downarrow$	-3.58	-1.72	-2.59	-2.52	-2.19	-2.25	-1.45	-1.58	-2.52	-1.67	-7.04	-4.57	+0.24	+0.30	-6.35	-4.68	+0.02	-0.98	-1.95	-4.84	-6.12	-0.84	-2.68		
LTP	Acc. ( $\Delta\%$ ) $\downarrow$	-8.71	-9.52	-8.45	-10.24	-4.62	-10.00	-5.59	-9.60	-9.57	-11.71	-5.57	-5.93	-0.31	-0.62	-6.49	+0.03	-1.69	-4.19	-2.75	-11.37	+3.10	-4.74	-5.84		
w/ Ours	FR ( $\Delta\%$ ) $\uparrow$	+11.11	+11.92	+10.87	+12.92	+5.90	+12.27	+8.04	+15.83	+11.89	+17.26	+6.55	+7.50	+0.45	+0.66	+7.63	+0.49	+2.09	+5.90	+3.51	+14.05	-3.56	+5.63	+7.68		
	ACR ( $\Delta\%$ ) $\downarrow$	+9.53	+10.58	+9.35	+11.30	+5.32	+10.70	+6.93	+12.25	+11.65	+14.33	+6.15	+6.54	+0.58	+0.72	+7.30	+0.41	+2.40	+6.03	+3.54	+12.96	-3.20	+5.95	+6.88		
BIA [86]	Acc. ( $\Delta\%$ ) $\downarrow$	-1.65	-1.31	-1.48	-1.85	-0.53	-2.01	-0.72	-1.71	-0.76	-2.00	-1.01	-0.77	+0.17	-0.47	-1.98	+2.42	+0.36	-0.20	-0.44	-1.83	+1.49	-0.50	-0.76		
w/ Ours	FR ( $\Delta\%$ ) $\uparrow$	+2.23	+1.99	+1.29	+0.01	-3.72	-1.59	-3.28	-2.85	-0.40	-2.33	-2.70	-0.94	-0.67	-0.25	-11.99	-1.34	-0.40	-1.08	-1.50	-4.32	-2.53	0.00	-2.16		
	ACR ( $\Delta\%$ ) $\downarrow$	+2.83	+2.46	+1.64	+0.05	+4.55	+1.96	+4.67	+4.80	+0.57	+3.67	+3.14	+1.22	+0.84	0.37	+14.30	+1.42	+0.53	+1.59	+2.06	+5.27	+2.92	0.01	+2.76		
GAMA	Acc. ( $\Delta\%$ ) $\downarrow$	-0.45	-0.36	-0.28	-0.09	-1.09	-0.27	-0.54	-0.39	+0.23	-0.54	-0.69	-0.04	-0.08	+0.13	-2.88	-1.00	+0.30	+0.10	+0.16	-0.92	-1.17	-0.06	-0.45		
w/ Ours	FR ( $\Delta\%$ ) $\uparrow$	+2.54	+2.46	+2.65	-2.15	-2.49	-2.19	-0.24	-0.17	-0.97	-1.84	-2.49	-2.94	+0.28	-0.06	+1.26	-0.23	-0.13	-0.44	-0.15	-0.94	-1.03	-1.32	-1.18		
	ACR ( $\Delta\%$ ) $\downarrow$	+3.22	+3.14	+3.40	+2.82	+3.14	+2.73	+0.34	+0.30	+1.22	+2.69	+2.92	+3.67	-0.36	+0.06	-1.51	+0.22	+0.10	+0.55	+0.19	+1.15	+1.27	+1.57	+1.49		
PDCL	Acc. ( $\Delta\%$ ) $\downarrow$	-0.73	+0.31	-1.26	+0.56	+0.46	+1.19	+1.64	+0.07	+1.30	-0.28	+0.83	-0.96	-0.22	-0.12	-0.58	+0.41	-0.32	+0.04	-0.02	-1.76	-2.48	+0.31	-0.85		
w/ Ours	FR ( $\Delta\%$ ) $\uparrow$	+2.81	+2.87	+2.91	+2.56	+2.76	+2.53	+0.24	+0.21	+1.20	+2.30	+2.67	+3.23	-0.25	+0.07	-1.29	+0.18	+0.12	+0.62	+0.16	+1.12	+1.14	+1.49	+1.35		
	ACR ( $\Delta\%$ ) $\downarrow$	-0.58	-0.14	-0.51	-0.08	-0.43	-0.31	-0.03	-0.02	-0.37	-0.49	-0.56	+0.03	-0.01	-0.27	-0.28	-0.39	-0.19	-0.04	-0.19	-0.16	-0.09	-0.09	-0.20		
FACL	Acc. ( $\Delta\%$ ) $\downarrow$	+0.10	-0.59	-3.35	-1.97	-4.92	-0.60	-3.29	-0.69	-2.01	-2.37	-1.91	-2.64	-0.80	-0.54	+0.15	-0.93	-0.39	-1.47	+4.03	+4.34	-3.22	-5.06	-1.28		
w/ Ours	FR ( $\Delta\%$ ) $\uparrow$	-0.20	+0.74	+4.30	+2.46	+6.15	+0.75	+4.68	+1.25	+2.40	+3.47	+2.23	+3.15	+0.95	+0.57	-0.16	+1.09	+0.43	+2.16	-0.81	-7.41	-6.81	+1.59	+1.32		
	ACR ( $\Delta\%$ ) $\downarrow$	-0.20	+0.64	+3.75	+2.27	+5.37	+0.74	+3.97	+0.96	+2.24	+3.04	+2.05	+2.78	+1.00	+0.61	-0.04	+1.32	+0.48	+2.04	-3.32	-4.93	+1.93	+3.51	+1.37		
PDCL	Acc. ( $\Delta\%$ ) $\downarrow$	+0.55	-0.29	+1.01	-0.40	-0.31	-0.98	-1.13	-0.06	-1.09	+0.22	-0.72	+0.79	+0.20	+0.16	+0.49	-0.36	+0.25	-0.05	+0.00	+1.41	+2.06	-0.28	-0.07	-0.85	
w/ Ours	FR ( $\Delta\%$ ) $\uparrow$	+0.68	+0.27	+1.08	+0.36	+0.45	+1.09	+1.42	+0.13	+1.23	-0.14	+0.81	-0.88	-0.41	-0.12	-0.40	+0.42	-0.31	-0.02	-0.07	-1.63	-2.32	+0.35	-0.07		
	ACR ( $\Delta\%$ ) $\downarrow$	+0.03	-0.18	+0.29	+0.09	+0.18	-0.22	-0.12	-0.05	-0.33	+0.13	-0.22	+0.21	+0.18	+0.25	+0.16	-0.18	-0.06	-0.08	-0.03	+0.19	+0.54	-0.11	+0.03		

Table 2: **Quantitative cross-domain transferability results.** We report the average improvement ( $\Delta\%$ ) with ours added from each baseline for each domain, in **gray row**. Better results in **boldface**.

Cross-domain		CUB-200-2011 [67]				Stanford Cars [33]				FGVC Aircraft [45]				Avg. Acc.
Method	Metric	Acc. $\downarrow$	ASR $\uparrow$	FR $\uparrow$	ACR $\downarrow$	Acc. $\downarrow$	ASR $\uparrow$	FR $\uparrow$	ACR $\downarrow$	Acc. $\downarrow$	ASR $\uparrow$	FR $\uparrow$	ACR $\downarrow$	
Benign	Acc. $\downarrow$	86.91	N/A	N/A	N/A	93.56	N/A	N/A	N/A	92.07	N/A	N/A	N/A	90.85
CDA [50]	Acc. ( $\Delta\%$ ) $\downarrow$	67.73	21.48	14.16	26.66	77.68	21.88	15.38	24.07	64.42	27.51	14.55	31.13	69.94
w/ Ours	FR ( $\Delta\%$ ) $\uparrow$	-16.92	+21.48	+20.63	-3.94	-5.86	+2.38	+2.35	-0.24	-22.58	+27.74	+26.44	-6.00	-15.12
LTP [33]	Acc. ( $\Delta\%$ ) $\downarrow$	-48.74	-43.32	-8.75	-49.31	-57.98	-39.02	-13.03	-40.87	-43.01	-54.15	-3.35	-56.48	-49.91
w/ Ours	FR ( $\Delta\%$ ) $\uparrow$	-10.43	+11.72	+10.87	-0.90	-10.62	+10.98	+10.68	-2.16	-6.41	+6.66	+6.35	-1.41	-9.15
BIA [86]	Acc. ( $\Delta\%$ ) $\downarrow$	-47.92	-46.13	-8.54	-50.26	-59.89	-37.22	-13.96	-38.97	-45.38	-51.52	-9.24	-54.06	-51.07
w/ Ours	FR ( $\Delta\%$ ) $\uparrow$	-0.02	+0.08	+0.09	0.49	-6.89	+6.89	+6.70	-2.00	-4.98	+5.25	+4.89	-1.24	-3.96
GAMA [11]	Acc. ( $\Delta\%$ ) $\downarrow$	-48.72	-45.41	-9.51	-49.67	-54.59	-42.58	-11.94	-44.28	-42.37	-54.46	-7.49	-56.77	-48.56
w/ Ours	FR ( $\Delta\%$ ) $\uparrow$	-2.41	+0.89	+2.30	-0.67	-2.33	+2.24	+2.10	-0.69	-2.68	+3.06	+2.87	0.14	-2.47
FACL [33]	Acc. ( $\Delta\%$ ) $\downarrow$	-40.85	-54.36	-7.21	-58.01	-51.23	-48.23	-12.9	-49.71	-40.08	-59.35	-7.34	-61.39	-44.05
w/ Ours	FR ( $\Delta\%$ ) $\uparrow$	+3.12	-3.79	-3.58	-0.70	-7.26	+2.34	+4.72	-4.49	-2.68	+0.60	+0.66	-0.24	-2.27
PDCL [83]	Acc. ( $\Delta\%$ ) $\downarrow$	-42.36	-52.32	-7.48	-55.93	-50.41	-46.83	-12.31	-48.46	-38.96	-58.23	-6.86	-60.34	-43.91
w/ Ours	FR ( $\Delta\%$ ) $\uparrow$	-0.46	+0.61	+0.66	0.40	-0.71	+0.75	+0.69	-0.32	-1.38	+1.52	+1.42	0.14	-0.85

Table 3: **Quantitative cross-task transferability results.** We report the average improvement ( $\Delta\%$ ) for our components applied to different generator architectures and evaluated against semantic segmentation (mIoU  $\downarrow$ ) and object detection (mAP50  $\downarrow$ ) models. MT denotes mean teacher, and better results in **boldface**.

Cross-task		Generator Arch.					
Method	Benign	U-Net			ResNet		
		Baseline	+MT	+MT+ $\mathcal{L}_{distill}$	Baseline	+MT	+MT+ $\mathcal{L}_{distill}$
DeepLabV3+ [11]	76.21	24.22	+0.76	<b>-2.92</b>	23.89	<b>-0.79</b>	<b>-1.84</b>
SegFormer [78]	71.89	29.34	<b>-3.31</b>	<b>-3.81</b>	25.60	<b>-0.78</b>	<b>-0.85</b>
Avg.	74.05	26.78	<b>-1.27</b>	<b>-3.36</b>	24.75	<b>-0.79</b>	<b>-1.35</b>
FRCNN [20]	61.01	27.51	<b>-0.05</b>	<b>-0.12</b>	28.43	+0.03	<b>-0.09</b>
DETR [8]	62.36	23.92	<b>-3.18</b>	<b>-3.54</b>	21.01	<b>-0.02</b>	<b>-0.29</b>
Avg.	61.69	25.72	<b>-1.62</b>	<b>-1.83</b>	24.72	+0.01	<b>-0.20</b>

to a single scale, preventing a fair comparison across attacks and undermining statistical significance. Third, evaluations in prior works commonly target a narrow set of victim architectures (e.g., mostly CNN-based), lacking the diversity of modern model families, including vision transformers (ViTs) and state-space models (SSMs), and thus overstating robustness. To address these shortcomings, we introduce the Accidental Correction Rate (ACR) as a complementary metric that captures the proportion of adversarial inputs that inadvertently restore correct predictions, enriching the assessment of attack efficacy alongside conventional measures (*i.e.*, ASR, FR, Accuracy).

We evaluate the effectiveness and transferability of adversarial attacks across model architectures and domain shifts using four key metrics. For notational convenience, let  $f(x)$  denote the predicted label for input  $x$ ,  $f(x + \delta)$  the prediction after applying adversarial perturbation  $\delta$ , and  $y$  the ground-truth label. The evaluation set is denoted by  $\mathcal{D}$ , with  $\mathcal{C} = \{x \in \mathcal{D} \mid f(x) = y\}$  representing correctly classified samples, and  $\mathcal{I} = \{x \in \mathcal{D} \mid f(x) \neq y\}$  denoting misclassified samples under clean inference. We formally define our evaluation metrics as follows:

$$\text{Accuracy}(\%) = \frac{|\{x \in \mathcal{D} \mid f(x + \delta) = y\}|}{|\mathcal{D}|}, \quad \text{ASR}(\%) = \frac{|\{x \in \mathcal{C} \mid f(x) = y \wedge f(x + \delta) \neq y\}|}{|\mathcal{C}|}, \quad (5)$$

$$\text{FR}(\%) = \frac{|\{x \in \mathcal{D} \mid f(x) \neq f(x + \delta)\}|}{|\mathcal{D}|}, \quad \text{ACR}(\%) = \frac{|\{x \in \mathcal{I} \mid f(x) \neq y \wedge f(x + \delta) = y\}|}{|\mathcal{I}|},$$

where *Top-1 Accuracy* [86, 82, 83] measures the overall proportion of correctly classified samples under clean or adversarial conditions. It serves as a global performance indicator to assess degraded performance after the attack, orthogonal to FR, ASR, and ACR. *Attack Success Rate (ASR)* [51, 50] is a subset of FR, which measures the proportion of originally correctly classified samples that are turned into misclassified ones by the adversarial attack. It directly reflects targeted misclassification. *Fooling Rate (FR)* [29, 48] quantifies the proportion of adversarial examples that cause a change in the model’s prediction, regardless of correctness. It reflects how often the attack disrupts the original decision and is used as transferability. *Accidental Correction Rate (ACR)*, also a subset of FR, is a novel metric that quantifies how often misclassified samples are “accidentally” corrected by

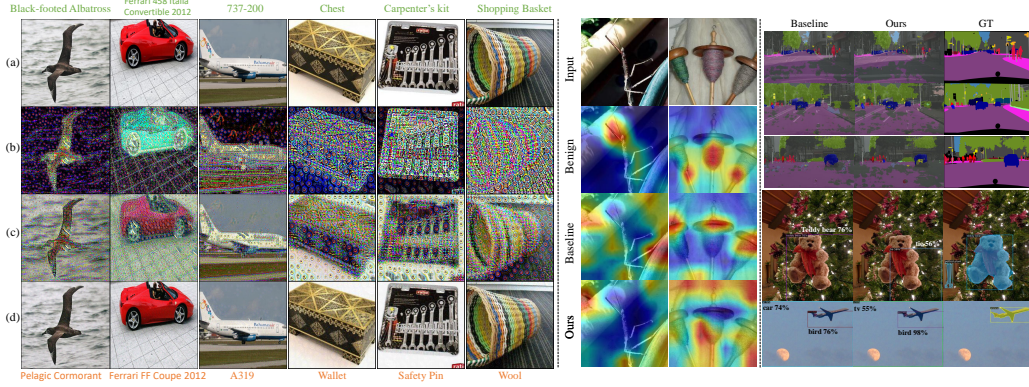


Figure 4: **Qualitative results.** Our semantic structure-aware attack successfully guides the generator to focus perturbations particularly on the semantically salient regions, effectively fooling the victim classifier. *Left:* (a) benign input image, (b) generated perturbation (normalized for visual purposes only), (c) unbounded adversarial image, and (d) bounded adversarial image across CUB-200-2011 [67], Stanford Cars [33], FGVC Aircraft [45], and ImageNet-1K [55] domains. The label on top (green) and bottom (orange) denotes the correct label and prediction after the attack, respectively. *Center:* We highlight that our method induces Grad-CAM [56] to focus on *drastically different regions* in our adversarial examples compared to both the benign image and the adversarial examples crafted by the baseline [86]. Moreover, our approach *noticeably spreads and reduces the high activation regions* observed in the benign and baseline cases, enhancing the transferability of our adversarial perturbations. *Right:* Cross-task prediction results (SS on top, OD on bottom). Our approach further disrupts the victim models by triggering higher false positive rates and wrong class label predictions. Please see the Appendix for more.

Table 4: **Comparison of cross-setting attack performance and image perceptual quality of AEs** We report the top-1 accuracy (%), mIoU, and mAP50 for classification, semantic segmentation, and object detection, respectively.

Method	Cross-setting (Avg.)				Perceptual Quality		
	Domain	Model	Task (SS)	Task (OD)	PSNR $\uparrow$	SSIM $\uparrow$	LPIPS $\downarrow$
CDA [50]	69.94	51.64	22.90	29.54	29.11	0.78	0.43
w/ Ours	<b>54.82</b>	<b>40.37</b>	<b>22.75</b>	<b>28.83</b>	29.17 (+0.06)	0.78 (-)	0.43 (-)
LTP [29]	49.91	50.14	25.34	25.90	29.11	0.76	0.47
w/ Ours	<b>44.51</b>	<b>44.30</b>	<b>24.48</b>	<b>24.52</b>	29.26 (+0.15)	0.77 (+0.01)	0.49 (+0.02)
BIA [86]	51.07	48.02	24.75	<b>24.52</b>	28.08	0.75	0.49
w/ Ours	<b>47.10</b>	<b>45.86</b>	<b>23.40</b>	<b>24.52</b>	28.76 (+0.68)	0.75 (-)	0.49 (-)
GAMA [1]	48.56	46.52	25.82	24.36	28.62	0.74	0.49
w/ Ours	<b>46.09</b>	<b>45.34</b>	<b>24.81</b>	<b>24.20</b>	28.69 (+0.07)	0.74 (-)	0.49 (-)
FACL [82]	44.05	44.26	25.08	24.43	28.61	0.74	0.49
w/ Ours	<b>42.98</b>	<b>41.01</b>	<b>24.20</b>	<b>23.97</b>	28.67 (+0.06)	0.74 (-)	0.49 (-)
PDCL [83]	43.91	45.02	25.24	24.93	28.68	0.74	0.48
w/ Ours	<b>43.06</b>	<b>45.08</b>	<b>24.20</b>	<b>24.20</b>	28.70 (+0.02)	0.74 (-)	0.49 (-)

Table 5: **Attack performance by varying test-time perturbation budget,  $\ell_\infty \leq \epsilon_{\text{test}}$ .** Our method improves the attack across all four settings even with an increased perturbation budget,  $\epsilon_{\text{test}}$ .

Method	Cross-setting (Avg.)	$\epsilon_{\text{test}} = 2$	4	6	8	10	16
Baseline [86]	Domain (Cls.; %)	90.15	87.35	78.73	64.95	51.07	24.87
	Model (Cls.; %)	74.84	71.42	64.63	56.11	45.44	31.79
	Task (SS; mIoU)	69.34	55.62	41.92	32.38	24.75	10.81
	Task (OD; mAP50)	49.90	44.08	37.60	30.96	24.72	13.69
w/ Ours	Domain (Cls.; %)	89.93	84.95	74.09	60.13	<b>47.10</b>	23.00
	Model (Cls.; %)	74.67	70.34	62.63	53.82	<b>43.46</b>	30.29
	Task (SS; mIoU)	69.10	54.95	40.84	31.28	<b>23.40</b>	10.00
	Task (OD; mAP50)	49.72	43.84	37.20	30.65	<b>24.52</b>	11.75

Table 6: **Ablation study on our proposed components.**

#	$\mathcal{L}_{adv}$	MT	$\mathcal{L}_{distill}$	U-Net		ResNet	
				Cross-domain	Cross-model	Cross-domain	Cross-model
1	✓	✗	✗	53.89	46.69	51.07	48.02
2	✓	✓	✗	51.20	46.11	47.91	46.02
3	✓	✓	✓	<b>49.03</b>	<b>45.41</b>	<b>47.10</b>	<b>45.86</b>

adversarial perturbations. This unintended side effect provides insight into model uncertainty and boundary behavior. For SS and OD tasks, we use the standard mIoU and mAP50 metrics, respectively.

### 4.3 Experimental Results

Table S5 reports cross-model evaluations across diverse architectures. As shown, augmenting each baseline generative attack with our method yields consistent improvements in attack success. While these results confirm the orthogonality and efficacy of our framework, we observe that CLIP-based approaches with objectives akin to ours, *e.g.* PDCL-Attack [83], yield only marginal improvements when combined with our method. We conjecture that optimizing for divergence in CLIP’s high-dimensional semantic embedding space may override or dilute the local structural consistency enforced by our early-block feature distillation, thereby attenuating the incremental gains from preserving fine-grained object contours and textures. Table 2 presents cross-domain transfer results. Incorporating our Mean Teacher smoothing and early-block distillation consistently enhances performance across unseen domains and architectures, demonstrating the broad applicability of our framework beyond the source data distribution. Table 3 evaluates transfer to SS and OD tasks, which were not seen during training. Even in these settings, our feature-distillation loss applied to the



Table 7: Ablation study on our feature distillation strategy. Our early intermediate block feature distillation strategy outperforms distilling other block features from teacher  $\mathcal{G}_{\theta'}$  to student  $\mathcal{G}_{\theta}$ .

Intermediate Block Features ( $\mathcal{G}_{\theta'} \rightarrow \mathcal{G}_{\theta}$ )				
	Early	Mid	Late	All
Ours (Best, runner-up)	Cross-domain Avg. (%)			
	47.10	50.95	49.03	51.13
	Cross-model Avg. (%)			
	45.86	48.07	47.59	49.44
	Cross-task (SS) Avg. (msd)			
	23.40	24.10	22.82	23.92
	Cross-task (OD) Avg. (msd)			
	24.52	24.53	24.69	24.52

Mean Teacher generator produces measurable gains. We attribute this cross-task generalization to our label-agnostic training pipeline and further validate that our method can be integrated with alternative generator architectures beyond ResNet. Qualitative results in Fig. 4 further confirm that our method produces more pronounced adversarial effects on target objects. See details on U-Net in the Appendix.

As shown in Table 5, across a range of  $\epsilon$  values, our method consistently enhances baseline transfer rates in all four cross-settings. These results demonstrate robustness to the choice of perturbation magnitude. Table 4 compares the cross-setting results and perceptual quality of the crafted AEs by method, where ours on top of each baseline maintains image quality on par with the baseline while achieving higher transferability across all cross-settings. This insinuates that since we encourage tighter semantic consistency within the generator, we do not observe perceptual distortions in PSNR, which can be seen from one method to another (*e.g.* LTP  $\rightarrow$  BIA). We report our results against adversarially trained models and input pre-processing defensive mechanisms in Table 8, where our method achieves superior attacks against the robust models compared to the baseline. These results confirm that enforcing semantic consistency in early generator blocks not only boosts transferability in standard black-box settings but also produces perturbations capable of further enhancing attacks against defense mechanisms. By anchoring structural cues in the early stages, our feature-distillation loss guides later blocks to synthesize noise that particularly targets semantically salient regions, yielding more potent and robust attacks against adversarially trained models and pre-processing defenses alike.

**Component-wise ablation study.** Table 6 compares three variants: baseline and our components added sequentially. Despite the different network architecture and the number of distilled block features, incorporating MT yields a clear improvement in transferability across both U-Net and ResNet, demonstrating that EMA smoothing alone can also regularize intermediate features and reduce noise. Adding our feature distillation loss then produces an additional performance gain, confirming that explicit semantic alignment in early blocks complements the implicit smoothing of MT and is crucial for crafting highly transferable perturbations.

**Block-wise ablation study.** Table 7 shows results when feature distillation loss is applied to different intermediate blocks. Distilling only the *early* block consistently yields the best performance in most cross-settings, hinting that our *early*-block semantic consistency is the most effective. Mid- and late-block distillation yield smaller gains, and distilling *all* blocks fails to match the early-block optimum. These results validate our key insight: early blocks consistently preserve the semantic structure the most out of the intermediate blocks, and anchoring perturbation synthesis there guides later layers to focus noise on object-centric regions, maximizing transferability.

## 5 Conclusion

In this paper, we introduce a semantic structure-aware generative attack that leverages a Mean Teacher framework and early-block feature distillation to preserve object contours, textures, and shapes, thereby guiding perturbations onto object-centric regions and markedly improving black-box transferability. Through our extensive experiments from diverse perspectives, we validate our approach to retaining object-salient regions in the image to boost adversarial transferability. Future work could involve advanced extensions of this mechanism to further enhance adversarial robustness and generalization.

Table 8: Superior attack success with our method against defenses, *i.e.*, Adversarially trained (AT) models and robust input pre-processing defense methods. Better results in **boldface**.

Method	Metric	Adv.Inc-V3	Adv.ViT	Adv.ConvNeXt	JPEG	BDR	R&P	Avg.
Clean	Acc. (%) $\downarrow$	76.33	48.82	58.44	74.68	74.68	76.58	68.26
Baseline [86]	Acc. (%) $\downarrow$	68.54	45.64	53.88	63.49	47.82	44.78	54.03
	ASR (%) $\uparrow$	14.95	11.72	10.26	20.24	40.76	44.59	23.75
	FR (%) $\uparrow$	24.02	25.48	19.40	28.09	48.06	51.60	32.78
	ACR (%) $\downarrow$	15.30	4.96	3.46	11.45	11.30	10.56	9.51
w/ Ours	Acc. (%) $\downarrow$	67.92	45.33	53.62	60.83	44.07	39.01	51.80
	ASR (%) $\uparrow$	15.75	11.95	10.65	23.74	45.37	51.63	26.52
	FR (%) $\uparrow$	24.83	25.31	19.60	31.61	52.22	57.86	35.28
	ACR (%) $\downarrow$	15.23	4.57	3.38	11.48	10.29	9.08	9.01



## References

- [1] A. Aich, C.-K. Ta, A. Gupta, C. Song, S. Krishnamurthy, S. Asif, and A. Roy-Chowdhury. Gama: Generative adversarial multi-object scene attacks. *Advances in Neural Information Processing Systems*, 35: 36914–36930, 2022. 2, 3, 4, 5, 6, 7, 8, 1, 9, 10
- [2] S. Baluja and I. Fischer. Adversarial transformation networks: Learning to generate adversarial examples. *arXiv preprint arXiv:1703.09387*, 2017. 2
- [3] S. Baluja and I. Fischer. Learning to attack: Adversarial transformation networks. In *Proceedings of the AAAI Conference on Artificial Intelligence*, volume 32, 2018. 2
- [4] H. Bao, L. Dong, S. Piao, and F. Wei. Beit: Bert pre-training of image transformers. *arXiv preprint arXiv:2106.08254*, 2021. 6, 5
- [5] J. Byun, S. Cho, M.-J. Kwon, H.-S. Kim, and C. Kim. Improving the transferability of targeted adversarial examples through object-based diverse input. In *Proceedings of the IEEE/CVF Conference on Computer Vision and Pattern Recognition*, pages 15244–15253, 2022. 5
- [6] H. Cai, J. Li, M. Hu, C. Gan, and S. Han. Efficientvit: Multi-scale linear attention for high-resolution dense prediction. *arXiv preprint arXiv:2205.14756*, 2022. 6, 5
- [7] S. Cao, D. Joshi, L.-Y. Gui, and Y.-X. Wang. Contrastive mean teacher for domain adaptive object detectors. In *Proceedings of the IEEE/CVF conference on computer vision and pattern recognition*, pages 23839–23848, 2023. 5
- [8] N. Carion, F. Massa, G. Synnaeve, N. Usunier, A. Kirillov, and S. Zagoruyko. End-to-end object detection with transformers. In *European conference on computer vision*, pages 213–229. Springer, 2020. 6, 7, 5
- [9] N. Carlini, A. Athalye, N. Papernot, W. Brendel, J. Rauber, D. Tsipras, I. Goodfellow, A. Madry, and A. Kurakin. On evaluating adversarial robustness. *arXiv preprint arXiv:1902.06705*, 2019. 2, 3
- [10] M. Caron, H. Touvron, I. Misra, H. Jégou, J. Mairal, P. Bojanowski, and A. Joulin. Emerging properties in self-supervised vision transformers. In *Proceedings of the IEEE/CVF international conference on computer vision*, pages 9650–9660, 2021. 5
- [11] L.-C. Chen, Y. Zhu, G. Papandreou, F. Schroff, and H. Adam. Encoder-decoder with atrous separable convolution for semantic image segmentation. In *Proceedings of the European conference on computer vision (ECCV)*, pages 801–818, 2018. 6, 7, 5
- [12] M. Cordts, M. Omran, S. Ramos, T. Rehfeld, M. Enzweiler, R. Benenson, U. Franke, S. Roth, and B. Schiele. The cityscapes dataset for semantic urban scene understanding. In *Proceedings of the IEEE conference on computer vision and pattern recognition*, pages 3213–3223, 2016. 6
- [13] J. Deng, W. Li, Y. Chen, and L. Duan. Unbiased mean teacher for cross-domain object detection. In *Proceedings of the IEEE/CVF conference on computer vision and pattern recognition*, pages 4091–4101, 2021. 5
- [14] M. Döbler, R. A. Marsden, and B. Yang. Robust mean teacher for continual and gradual test-time adaptation. In *Proceedings of the IEEE/CVF Conference on Computer Vision and Pattern Recognition*, pages 7704–7714, 2023. 5
- [15] Y. Dong, F. Liao, T. Pang, H. Su, J. Zhu, X. Hu, and J. Li. Boosting adversarial attacks with momentum. In *Proceedings of the IEEE conference on computer vision and pattern recognition*, pages 9185–9193, 2018. 2, 1
- [16] Y. Dong, T. Pang, H. Su, and J. Zhu. Evading defenses to transferable adversarial examples by translation-invariant attacks. In *Proceedings of the IEEE/CVF Conference on Computer Vision and Pattern Recognition*, pages 4312–4321, 2019. 3
- [17] Y. Dong, T. Pang, H. Su, and J. Zhu. Evading defenses to transferable adversarial examples by translation-invariant attacks. In *Proceedings of the IEEE Computer Society Conference on Computer Vision and Pattern Recognition*, 2019. 2, 1
- [18] A. Dosovitskiy, L. Beyer, A. Kolesnikov, D. Weissenborn, X. Zhai, T. Unterthiner, M. Dehghani, M. Minderoeder, G. Heigold, S. Gelly, J. Uszkoreit, and N. Houlsby. An image is worth 16x16 words: Transformers for image recognition at scale. *ICLR*, 2021. 6, 5
- [19] T. Furlanello, Z. Lipton, M. Tschannen, L. Itti, and A. Anandkumar. Born again neural networks. In *International conference on machine learning*, pages 1607–1616. PMLR, 2018. 4

- [20] R. Girshick. Fast r-cnn. In *Proceedings of the IEEE international conference on computer vision*, pages 1440–1448, 2015. 6, 7, 5
- [21] J.-B. Grill, F. Strub, F. Altché, C. Tallec, P. Richemond, E. Buchatskaya, C. Doersch, B. Avila Pires, Z. Guo, M. Gheshlaghi Azar, et al. Bootstrap your own latent—a new approach to self-supervised learning. *Advances in neural information processing systems*, 33:21271–21284, 2020. 5
- [22] C. Guo, M. Rana, M. Cisse, and L. Van Der Maaten. Countering adversarial images using input transformations. *arXiv preprint arXiv:1711.00117*, 2017. 6
- [23] A. Hatamizadeh and J. Kautz. Mambavision: A hybrid mamba-transformer vision backbone. In *Proceedings of the Computer Vision and Pattern Recognition Conference*, pages 25261–25270, 2025. 6, 5
- [24] K. He, X. Zhang, S. Ren, and J. Sun. Deep residual learning for image recognition. In *CVPR*, 2016. 6, 1, 4, 5
- [25] J. Hu, L. Shen, and G. Sun. Squeeze-and-excitation networks. In *Proceedings of the IEEE conference on computer vision and pattern recognition*, pages 7132–7141, 2018. 6, 4
- [26] G. Huang, Z. Liu, L. van der Maaten, and K. Q. Weinberger. Densely connected convolutional networks. In *CVPR*, 2017. 6, 5
- [27] Q. Huang, I. Katsman, H. He, Z. Gu, S. Belongie, and S.-N. Lim. Enhancing adversarial example transferability with an intermediate level attack. In *Proceedings of the IEEE/CVF international conference on computer vision*, pages 4733–4742, 2019. 5
- [28] F. N. Iandola, S. Han, M. W. Moskewicz, K. Ashraf, W. J. Dally, and K. Keutzer. Squeezenet: Alexnet-level accuracy with 50x fewer parameters and < 0.5 mb model size. *arXiv preprint arXiv:1602.07360*, 2016. 6, 5
- [29] K. kanth Nakka and M. Salzmann. Learning transferable adversarial perturbations. In A. Beygelzimer, Y. Dauphin, P. Liang, and J. W. Vaughan, editors, *Advances in Neural Information Processing Systems*, 2021. URL <https://openreview.net/forum?id=sIDvIyR5I1R>. 2, 3, 4, 6, 7, 8, 1, 9, 10
- [30] K. Kim, B. Ji, D. Yoon, and S. Hwang. Self-knowledge distillation with progressive refinement of targets. In *Proceedings of the IEEE/CVF international conference on computer vision*, pages 6567–6576, 2021. 4
- [31] W. J. Kim, S. Hong, and S.-E. Yoon. Diverse generative perturbations on attention space for transferable adversarial attacks. In *2022 IEEE international conference on image processing (ICIP)*, pages 281–285. IEEE, 2022. 5
- [32] D. P. Kingma and J. Ba. Adam: A method for stochastic optimization. In *ICLR*, 2015. 5
- [33] J. Krause, M. Stark, J. Deng, and L. Fei-Fei. 3d object representations for fine-grained categorization. In *2013 IEEE International Conference on Computer Vision Workshops*, pages 554–561, 2013. doi: 10.1109/ICCVW.2013.77. 6, 7, 8, 4, 5
- [34] A. Kurakin, I. Goodfellow, and S. Bengio. Adversarial machine learning at scale. *arXiv preprint arXiv:1611.01236*, 2016. 3, 6
- [35] Y. Lee, J. R. Willette, J. Kim, J. Lee, and S. J. Hwang. Exploring the role of mean teachers in self-supervised masked auto-encoders. In *The Eleventh International Conference on Learning Representations*, 2023. URL <https://openreview.net/forum?id=7sn6Vxp92xV>. 5
- [36] Q. Li, Y. Guo, W. Zuo, and H. Chen. Improving adversarial transferability via intermediate-level perturbation decay. *Advances in Neural Information Processing Systems*, 36:32900–32912, 2023. 5
- [37] Y.-J. Li, X. Dai, C.-Y. Ma, Y.-C. Liu, K. Chen, B. Wu, Z. He, K. Kitani, and P. Vajda. Cross-domain adaptive teacher for object detection. In *Proceedings of the IEEE/CVF conference on computer vision and pattern recognition*, pages 7581–7590, 2022. 5
- [38] Z. Li, X. Li, L. Yang, R. Song, J. Yang, and Z. Pan. Dual teachers for self-knowledge distillation. *Pattern Recognition*, 151:110422, 2024. 4
- [39] J. Lin, C. Song, K. He, L. Wang, and J. E. Hopcroft. Nesterov accelerated gradient and scale invariance for adversarial attacks. *arXiv preprint arXiv:1908.06281*, 2019. 3
- [40] T.-Y. Lin, M. Maire, S. Belongie, J. Hays, P. Perona, D. Ramanan, P. Dollár, and C. L. Zitnick. Microsoft coco: Common objects in context. In *Computer vision—ECCV 2014: 13th European conference, zurich, Switzerland, September 6–12, 2014, proceedings, part v 13*, pages 740–755. Springer, 2014. 6

- [41] Z. Liu, Y. Lin, Y. Cao, H. Hu, Y. Wei, Z. Zhang, S. Lin, and B. Guo. Swin transformer: Hierarchical vision transformer using shifted windows. In *Proceedings of the IEEE/CVF international conference on computer vision*, pages 10012–10022, 2021. 6, 5
- [42] Z. Liu, H. Mao, C.-Y. Wu, C. Feichtenhofer, T. Darrell, and S. Xie. A convnet for the 2020s. In *Proceedings of the IEEE/CVF conference on computer vision and pattern recognition*, pages 11976–11986, 2022. 5
- [43] A. Madry, A. Makelov, L. Schmidt, D. Tsipras, and A. Vladu. Towards deep learning models resistant to adversarial attacks. *arXiv preprint arXiv:1706.06083*, 2017. 2, 3
- [44] A. Madry, A. Makelov, L. Schmidt, D. Tsipras, and A. Vladu. Towards deep learning models resistant to adversarial attacks. *arXiv preprint arXiv:1706.06083*, 2017. 1
- [45] S. Maji, E. Rahtu, J. Kannala, M. B. Blaschko, and A. Vedaldi. Fine-grained visual classification of aircraft. *ArXiv*, abs/1306.5151, 2013. URL <https://api.semanticscholar.org/CorpusID:2118703>. 6, 7, 8, 4, 5
- [46] S. Marcel and Y. Rodriguez. Torchvision the machine-vision package of torch. In *Proceedings of the 18th ACM international conference on Multimedia*, pages 1485–1488, 2010. 6, 4, 5
- [47] S.-M. Moosavi-Dezfooli, A. Fawzi, O. Fawzi, and P. Frossard. Universal adversarial perturbations. In *Proceedings of the IEEE conference on computer vision and pattern recognition*, pages 1765–1773, 2017. 1
- [48] K. K. Nakka and A. Alahi. Nat: Learning to attack neurons for enhanced adversarial transferability. In *2025 IEEE/CVF Winter Conference on Applications of Computer Vision (WACV)*, pages 7593–7604. IEEE, 2025. 2, 3, 5, 6, 7, 1, 4
- [49] M. Naseer, S. Khan, M. Hayat, F. S. Khan, and F. Porikli. A self-supervised approach for adversarial robustness. In *Proceedings of the IEEE/CVF Conference on Computer Vision and Pattern Recognition*, pages 262–271, 2020. 9, 10
- [50] M. M. Naseer, S. H. Khan, M. H. Khan, F. Shahbaz Khan, and F. Porikli. Cross-domain transferability of adversarial perturbations. *Advances in Neural Information Processing Systems*, 32, 2019. 2, 3, 4, 6, 7, 8, 1, 9, 10
- [51] O. Poursaeed, I. Katsman, B. Gao, and S. Belongie. Generative adversarial perturbations. In *Proceedings of the IEEE conference on computer vision and pattern recognition*, pages 4422–4431, 2018. 2, 3, 6, 7, 1
- [52] A. Radford, J. W. Kim, C. Hallacy, A. Ramesh, G. Goh, S. Agarwal, G. Sastry, A. Askell, P. Mishkin, J. Clark, et al. Learning transferable visual models from natural language supervision. In *International conference on machine learning*, pages 8748–8763. PMLR, 2021. 3, 9, 10
- [53] I. Radosavovic, R. P. Kosaraju, R. Girshick, K. He, and P. Dollár. Designing network design spaces. In *Proceedings of the IEEE/CVF conference on computer vision and pattern recognition*, pages 10428–10436, 2020. 6, 5
- [54] O. Ronneberger, P. Fischer, and T. Brox. U-net: Convolutional networks for biomedical image segmentation. In *Medical image computing and computer-assisted intervention—MICCAI 2015: 18th international conference, Munich, Germany, October 5-9, 2015, proceedings, part III 18*, pages 234–241. Springer, 2015. 1, 2
- [55] O. Russakovsky, J. Deng, H. Su, J. Krause, S. Satheesh, S. Ma, Z. Huang, A. Karpathy, A. Khosla, M. S. Bernstein, A. C. Berg, and F. Li. Imagenet large scale visual recognition challenge. *IJCV*, 2015. 6, 8, 5
- [56] R. R. Selvaraju, M. Cogswell, A. Das, R. Vedantam, D. Parikh, and D. Batra. Grad-cam: Visual explanations from deep networks via gradient-based localization. In *Proceedings of the IEEE international conference on computer vision*, pages 618–626, 2017. 8, 5
- [57] N. D. Singh, F. Croce, and M. Hein. Revisiting adversarial training for imagenet: Architectures, training and generalization across threat models. In *NeurIPS*, 2023. 6
- [58] C. Szegedy, W. Zaremba, I. Sutskever, J. Bruna, D. Erhan, I. Goodfellow, and R. Fergus. Intriguing properties of neural networks. *arXiv preprint arXiv:1312.6199*, 2013. 1
- [59] C. Szegedy, V. Vanhoucke, S. Ioffe, J. Shlens, and Z. Wojna. Rethinking the inception architecture for computer vision. In *CVPR*, 2016. 6, 5

- [60] M. Tan and Q. Le. Efficientnetv2: Smaller models and faster training. arxiv 2021. *arXiv preprint arXiv:2104.00298*. 6, 5
- [61] M. Tan, B. Chen, R. Pang, V. Vasudevan, M. Sandler, A. Howard, and Q. V. Le. Mnasnet: Platform-aware neural architecture search for mobile. In *Proceedings of the IEEE/CVF conference on computer vision and pattern recognition*, pages 2820–2828, 2019. 6, 5
- [62] A. Tarvainen and H. Valpola. Mean teachers are better role models: Weight-averaged consistency targets improve semi-supervised deep learning results. *Advances in neural information processing systems*, 30, 2017. 4, 5, 6
- [63] I. O. Tolstikhin, N. Houlsby, A. Kolesnikov, L. Beyer, X. Zhai, T. Unterthiner, J. Yung, A. Steiner, D. Keysers, J. Uszkoreit, et al. Mlp-mixer: An all-mlp architecture for vision. *Advances in neural information processing systems*, 34:24261–24272, 2021. 6, 5
- [64] H. Touvron, M. Cord, M. Douze, F. Massa, A. Sablayrolles, and H. Jégou. Training data-efficient image transformers & distillation through attention. In *International conference on machine learning*, pages 10347–10357. PMLR, 2021. 6, 5
- [65] A. Trockman and J. Z. Kolter. Patches are all you need? *arXiv preprint arXiv:2201.09792*, 2022. 6, 5
- [66] Z. Tu, H. Talebi, H. Zhang, F. Yang, P. Milanfar, A. Bovik, and Y. Li. Maxvit: Multi-axis vision transformer. In *European conference on computer vision*, pages 459–479. Springer, 2022. 6
- [67] C. Wah, S. Branson, P. Welinder, P. Perona, and S. Belongie. The Caltech-UCSD Birds-200-2011 Dataset. Technical report, California Institute of Technology, 2011. 6, 7, 8, 4, 5
- [68] C. Wang, C. Xu, C. Wang, and D. Tao. Perceptual adversarial networks for image-to-image transformation. *IEEE Transactions on Image Processing*, 27(8):4066–4079, 2018. 2
- [69] J. Wang, K. Sun, T. Cheng, B. Jiang, C. Deng, Y. Zhao, D. Liu, Y. Mu, M. Tan, X. Wang, et al. Deep high-resolution representation learning for visual recognition. *IEEE transactions on pattern analysis and machine intelligence*, 43(10):3349–3364, 2020. 6, 5
- [70] R. Wang, Z. Wu, Z. Weng, J. Chen, G.-J. Qi, and Y.-G. Jiang. Cross-domain contrastive learning for unsupervised domain adaptation. *IEEE Transactions on Multimedia*, 2022. 3, 2
- [71] X. Wang, X. He, J. Wang, and K. He. Admix: Enhancing the transferability of adversarial attacks. In *Proceedings of the IEEE/CVF International Conference on Computer Vision*, pages 16158–16167, 2021. 3
- [72] R. Wightman. PyTorch Image Models. URL <https://github.com/huggingface/pytorch-image-models>. 6, 4, 5
- [73] W. Wu, Y. Su, X. Chen, S. Zhao, I. King, M. R. Lyu, and Y.-W. Tai. Boosting the transferability of adversarial samples via attention. In *Proceedings of the IEEE/CVF Conference on Computer Vision and Pattern Recognition*, pages 1161–1170, 2020. 5
- [74] C. Xiao, B. Li, J.-Y. Zhu, W. He, M. Liu, and D. Song. Generating adversarial examples with adversarial networks. *arXiv preprint arXiv:1801.02610*, 2018. 2, 1
- [75] C. Xie, J. Wang, Z. Zhang, Z. Ren, and A. Yuille. Mitigating adversarial effects through randomization. In *International Conference on Learning Representations*, 2018. URL <https://openreview.net/forum?id=Sk9yuql0Z>. 6
- [76] C. Xie, Z. Zhang, Y. Zhou, S. Bai, J. Wang, Z. Ren, and A. Yuille. Improving transferability of adversarial examples with input diversity. In *Computer Vision and Pattern Recognition*. IEEE, 2019. 2, 1
- [77] C. Xie, Z. Zhang, Y. Zhou, S. Bai, J. Wang, Z. Ren, and A. L. Yuille. Improving transferability of adversarial examples with input diversity. In *Proceedings of the IEEE/CVF conference on computer vision and pattern recognition*, pages 2730–2739, 2019. 3
- [78] E. Xie, W. Wang, Z. Yu, A. Anandkumar, J. M. Alvarez, and P. Luo. Segformer: Simple and efficient design for semantic segmentation with transformers. *Advances in neural information processing systems*, 34:12077–12090, 2021. 6, 7, 5
- [79] S. Xie, R. Girshick, P. Dollár, Z. Tu, and K. He. Aggregated residual transformations for deep neural networks. In *Proceedings of the IEEE conference on computer vision and pattern recognition*, pages 1492–1500, 2017. 5

- [80] W. Xu, D. Evans, and Y. Qi. Feature squeezing: Detecting adversarial examples in deep neural networks. In *NDSS*, 2018. doi: 10.14722/ndss.2018.23295. URL <https://www.ndss-symposium.org/ndss-paper/feature-squeezing-detecting-adversarial-examples-in-deep-neural-networks/>. 6
- [81] H. Yang, J. Jeong, and K.-J. Yoon. FacI-attack: Frequency-aware contrastive learning for transferable adversarial attacks. 2023. 2, 3, 6
- [82] H. Yang, J. Jeong, and K.-J. Yoon. FacI-attack: Frequency-aware contrastive learning for transferable adversarial attacks. In *Proceedings of the AAAI Conference on Artificial Intelligence*, volume 38, pages 6494–6502, 2024. 3, 4, 5, 6, 7, 8, 1, 2, 9, 10
- [83] H. Yang, J. Jeong, and K.-J. Yoon. Prompt-driven contrastive learning for transferable adversarial attacks. In *European Conference on Computer Vision*, pages 36–53. Springer, 2024. 2, 3, 4, 5, 6, 7, 8, 1, 9, 10
- [84] S. Yun, J. Park, K. Lee, and J. Shin. Regularizing class-wise predictions via self-knowledge distillation. In *The IEEE/CVF Conference on Computer Vision and Pattern Recognition (CVPR)*, June 2020. 4
- [85] C. Zhang, A. Karjauv, P. Benz, S. Ham, G. Cho, C.-H. Youn, and I. S. Kweon. Is fgsm optimal or necessary for  $l_\infty$  adversarial attack? In *Workshop on Adversarial Machine Learning in Real-World Computer Vision Systems and Online Challenges (AML-CV)*. Computer Vision Foundation (CVF), IEEE Computer Society, 2021. 2, 1
- [86] Q. Zhang, X. Li, Y. Chen, J. Song, L. Gao, Y. He, and H. Xue. Beyond imagenet attack: Towards crafting adversarial examples for black-box domains. In *International Conference on Learning Representations*, 2022. 2, 3, 4, 5, 6, 7, 8, 9, 1, 10
- [87] Y. Zhang, T. Xiang, T. M. Hospedales, and H. Lu. Deep mutual learning. In *Proceedings of the IEEE conference on computer vision and pattern recognition*, pages 4320–4328, 2018. 4
- [88] S. Zhao, J. Yu, Z. Sun, B. Zhang, and X. Wei. Enhanced accuracy and robustness via multi-teacher adversarial distillation. In *European Conference on Computer Vision*, pages 585–602. Springer, 2022. 5
- [89] L. Zhu, B. Liao, Q. Zhang, X. Wang, W. Liu, and X. Wang. Vision mamba: Efficient visual representation learning with bidirectional state space model. In *Forty-first International Conference on Machine Learning*, 2024. URL <https://openreview.net/forum?id=YbHCqn4qF4>. 6, 5



---

# Semantic Structure-Aware Generative Attacks for Enhanced Adversarial Transferability

---

## Supplementary Material

In this supplementary material, we provide comprehensive insights and detailed resources that complement our main manuscript. First, we provide an in-depth review of related work in Sec. A. We then highlight the distinctions of our method that clearly distinguish it from the concurrent works, describe the reason for enhanced adversarial transferability in Sec. B, and provide additional experimental details and results in Sec. C aimed at supplementing our manuscript for a better understanding of our approach.

## A Additional Related Work

**Iterative attacks.** For years, iterative gradient-based attacks have become a cornerstone of adversarial research. Methods such as Projected Gradient Descent (PGD) [44] extend the Fast Gradient Sign Method by applying multiple small,  $\ell_\infty$ -bounded steps; Momentum Iterative FGSM (MI-FGSM) [15] further stabilizes updates via accumulated momentum; Diverse Input FGSM (DI-FGSM) [76] injects random resizing and padding at each iteration; and Translation-Invariant FGSM (TI-FGSM) [17] averages gradients over shifted inputs to enhance spatial robustness. More advanced variants even incorporate feature-space objectives to target intermediate representations [85].

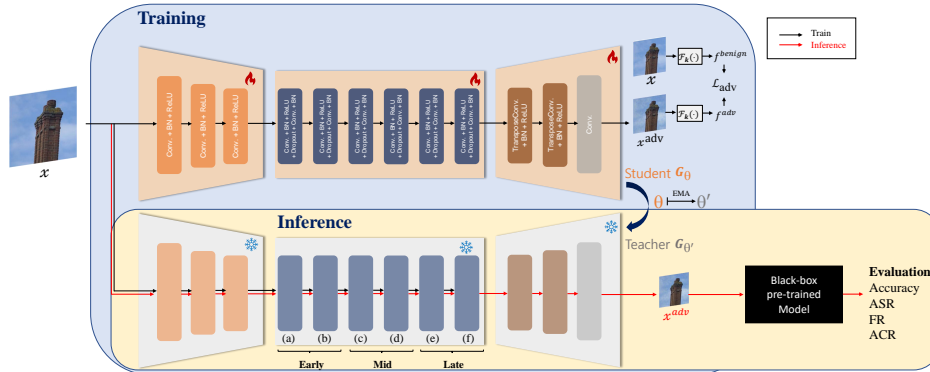
**Generative model-based attacks.** In parallel, more efficient generative model-based attacks train a feed-forward image-to-image transformation network to synthesize perturbations in a single pass: Universal Adversarial Perturbations (UAP) [47] learn a single image-agnostic noise vector, Generative Adversarial Perturbations (GAP) [51] use a GAN framework to produce highly transferable noise maps (added to the input images), and AdvGAN [74] leverages GANs for image-dependent attacks that balance stealth and speed. Together, these two paradigms offer complementary trade-offs between precision, transferability, and inference efficiency.

In this vein, recent generative model-based untargeted attack methods [50, 29, 86, 1, 82, 83, 48] have further added techniques to enhance the transferability of the crafted adversarial examples by incorporating surrogate model’s output logit-level and mid-level feature-level separation, frequency domain manipulation, vision-language model guidance, and heuristic selection of one effective neuron-level generator among a pool of multiple generators. However, none of these works have dealt with directly manipulating the generative feature space to improve the transferability of AEs. To address this, we uncover the correlation between generative features and adversarial transferability of the output AEs in this work.

**U-Net-based generator.** Along with ResNet [24], U-Net [54] is another effective network architecture comprising a symmetric encoder-decoder with skip connections, fusing low- and high-level features to preserve fine-grained details, which are ideal when perturbations must tightly follow object boundaries. By contrast, a ResNet generator stacks residual blocks with identity shortcuts, thus building deep hierarchical representations that emphasize global context. Although U-Net decoders add computational overhead, they can produce sharper, pixel-accurate noise, while ResNet backbones scale more efficiently and excel at generating broadly distributed perturbations. Ultimately, the choice of generator architecture hinges on the desired trade-off between pixel-level fidelity, attack transferability, and inference speed.

In the context of generative adversarial attack, GAP [51] first demonstrated that U-Net can serve as a perturbation generator with a lower inference time cost than that with ResNet. However, the authors of [51] also stated that ResNet, in general, outperforms U-Net in attack transferability. In this work, we demonstrate that our method of anchoring perturbation generation on early-intermediate features can also be applied to a different generator architecture than ResNet, namely U-Net [54].

## B Our method distinction from previous works



Our method stands distinct from the focus of existing generative attacks in that we delve into the generator feature space, rather than the surrogate model space, as categorized in Table S1. Previous works have targeted various stages of the generative attack pipeline [51, 50, 29, 86], including input data augmentation, pixel-level perturbation, surrogate model’s logit- and feature-level manipulations. Nonetheless, no work has yet explicitly manipulated the internal features of the generative model to enhance transferability. In this work, we investigate how internal feature representations within generative models can be harnessed to enhance the transferability of AEs.

Table S1: **Our method distinction.** Comparison of transfer-based generative adversarial attacks, highlighted by the method’s targeted stage in the training pipeline (in order from left to right), and GT label requirement.

Attack	Input data aug.	Generator feature-level	Perturbed image-level	Surrogate		GT label required?
				mid-level layer feature-level	Surrogate output logit-level	
GAP [51]	-	-	-	-	✓	-
CDA [70]	-	-	-	-	-	-
LTP [29]	-	-	✓	✓	-	-
BIA [86]	-	-	-	✓	-	-
GAMA [1]	-	-	-	✓	-	✓
FACL [82]	✓	-	-	✓	-	-
PDCL [83]	-	-	-	-	-	✓
Our focus	-	✓	-	-	-	-

Attack	Input data aug.	Generator feature-level	Surrogate		Surrogate	GT label required?
			Perturbed image-level	mid-level layer feature-level	output logit-level	
GAP [51]	-	-	-	-	✓	-
CDA [70]	-	-	-	-	✓	-
LTP [29]	-	-	-	-	-	-
BIA [86]	-	-	✓	✓✓✓	-	-
GAMA [1]	-	-	-	-	-	✓
FACL [82]	✓	-	-	✓✓✓	-	-
PDCL [83]	-	-	-	✓	-	✓
Our focus	-	✓	-	-	-	-

**Reason for transferability.** Our empirical analysis of intermediate feature activation maps from existing ResNet-based generators reveals that coarse, object-salient regions consistently emerge in the early residual blocks, and appear even more pronounced in models with higher black-box transferability. This insight suggests that these early-block features play a pivotal role in shaping perturbations. To capitalize on this, we anchor our adversarial noise generation to the clean image’s semantic structure at these early stages. Lacking explicit semantic priors to retain the semantic integrity of the benign input images, we introduce a Mean Teacher mechanism: by maintaining an exponential moving average (EMA) of the student generator’s weights, the teacher generator yields temporally smoothed features that are *largely free of adversarial noise*. We then fully leverage the Mean Teacher framework by further imposing a feature distillation loss between the student generator’s and the teacher’s early-intermediate block activations, *filtering out spurious noise while preserving the coarse object shapes and boundaries* present in the teacher generator features. This strict semantic-consistency constraint focuses perturbation power on object-salient regions, thereby enhancing transferability without sacrificing efficiency.

In the figure below (Fig. S2), we directly compare the feature activation maps and the added adversarial noise per block (absolute difference of the input and output of each block) of Ours against the baseline [86]. We particularly focus on the intermediate residual blocks (“Residual Learning”), as most of the adversarial noise is generated in these blocks [86], and the preceding (“Downsampling” layers) and succeeding blocks (“Upsampling” layers) serve to simply adjust the spatial resolution of the feature maps.

We preserve semantic integrity in the early blocks because these layers capture the coarse structure of the object, such as boundaries and shapes. By aligning the student model’s early block activations to a teacher reference, we remove incidental details and initial noise. This alignment compresses feature magnitudes and lowers the measured semantic quality in those early blocks. However, that simpler representation allows the generator to focus on stronger and more widespread noise in the later layers.

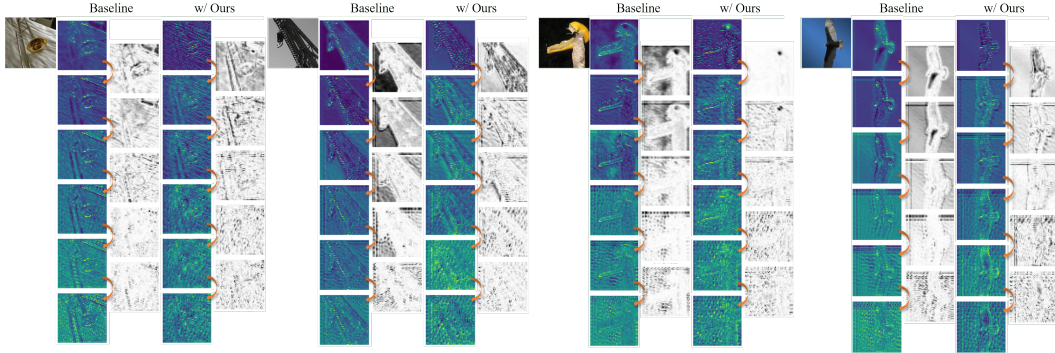


Figure S2: Comparison of the input image (column 1), the feature activation maps, and the added adversarial noise between two residual blocks (absolute difference between the feature maps of two residual blocks) of Ours (columns 4, 5) against the baseline [86] (columns 2, 3). Although the baseline’s feature maps more vividly emphasize object boundaries and contours, this focus actually prevents perturbations from appearing in those highlighted regions. By contrast, our method produces relatively less pronounced early features than those of the baseline, yet focuses more perturbation power on object-salient regions towards the later blocks than the baseline, thereby allowing adversarial noise to be dispersed directly on and around those salient regions, as opposed to the baseline. For the feature activation maps and the added noise, the brighter and darker (respectively), the higher the value.

**Deliberate compression of early features.** We enforce semantic consistency in the early blocks to focus the generator on true object outlines. Aligning student features to a smoothed teacher strips away incidental detail and any initial noise, which reduces the average magnitude of feature activations, and thus appears to degrade early-block semantics. That lean representation then lets the network concentrate its available capacity deeper in the intermediate blocks, where it produces stronger and more widely dispersed perturbations. When comparing the absolute difference between two feature maps in Fig. S2, we see that the baseline avoids object-salient regions and restricts noise to the peripheral regions, whereas our approach applies noise across the entire image, including the object itself. Although the early semantics seem more degraded relative to the baseline, this deliberate

compression of early features enables a broader attack on diverse features. Although the baseline’s early blocks may exhibit stronger semantic activations, our method’s slightly muted early features enable a broader and more effective perturbation distribution towards the later intermediate blocks, thus achieving higher transferability than the baseline. Crucially, we observe that *the baseline’s finely detailed early-block semantics add little benefit; retaining only the coarse semantic outline is sufficient to guide highly transferable perturbations*.

**Summary of our approach.** We further summarize our findings and approach as follows. We empirically discover that existing generative works preserve the semantic integrity of the benign input image at the early intermediate blocks better than the later blocks, under the assumption that the downsampling blocks merely serve as feature extractors [86]. To better structure adversarial noise generation in the intermediate blocks, we formulate our method to maintain at least coarse semantic structures in the *early* intermediate blocks, thereby yielding much more perturbed features towards the end of the intermediate stage, which then results in enhanced transferability of the crafted AEs compared to the baseline. Through extensive cross-setting evaluations, we validate our approach of tuning the progression of adversarial noise generation in the generator’s feature level as a compatible method to the existing generative attack framework [50, 29, 86, 1, 82, 83, 48] without much overheads.

### Comparison of feature activation maps by block.

Compared to the baseline and to ablations that apply distillation in mid layers, late layers, or across all layers, our approach of enforcing semantic consistency in the early block produces the most effective and transferable perturbations (Fig. S3). When we inspect feature activation maps, we see that preserving the coarse semantic structure in the earliest layers anchors the noise to object-salient regions that tend to be shared across different models. This focus prevents the generator from wasting capacity on irrelevant details and guides it to concentrate its attack on universally important features. By contrast, distillation applied later or across all intermediate blocks causes noise to be rather sparse or dispersed over regions away from those core cues, resulting in weaker transfer performance.

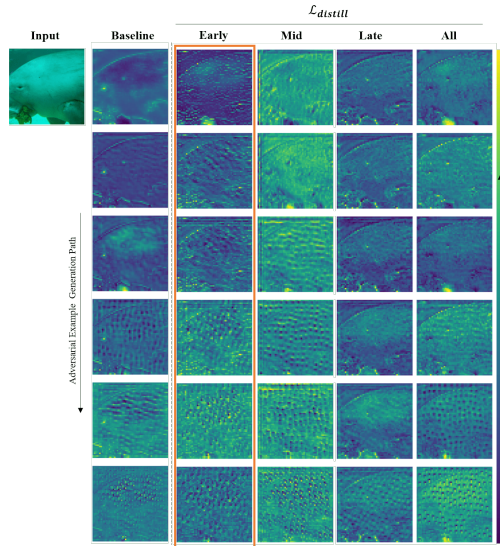


Figure S3: Comparison of feature activation maps by distilled block.

## C Experimental Details

### C.1 Details on the evaluation settings

We define three black-box evaluation scenarios that differ in the attacker’s knowledge of target data and models. In the cross-model setting, the adversary has access to the same data distribution used to train the unseen target models but must craft attacks using a substitute model rather than querying the targets directly. In the cross-domain setting, the attacker works solely with out-of-domain data and has no access to target-domain datasets (e.g., CUB-200-2011 [67], Stanford Cars [33], FGVC Aircraft [45]) or the ability to query target-domain models such as ResNet-50 [24], SE-Net, or SE-ResNet101 [25]. Finally, in the cross-task setting, likewise, the adversary is completely agnostic to the target’s data, models, and even the task itself, representing the strict black-box challenge.

**Victim model specifications.** we selected a total of 22 different model architectures that span from CNNs to Vision Mamba variants, whose pre-trained model weights are available openly through TorchVision [46], Timm [72], and the proprietary GitHub repositories. We list the sources in Table S2.

Table S2: Sources of victim models used to evaluate the attack performance, grouped by task.

Task	Victim Model	Source
Image Classification	ResNet50 [24]	TorchVision [46]
	ResNet152 [24]	TorchVision [46]
	Dense121 [26]	TorchVision [46]
	Dense169 [26]	TorchVision [46]
	InceptionV3 [59]	TorchVision [46]
	RegNetY [53]	TorchVision [46]
	MNASNet [61]	TorchVision [46]
	SqueezeNet [28]	TorchVision [46]
	EfficientV2 [60]	TorchVision [46]
	HRNet_W32 [69]	Timm [72]
	ConvNeXt [42]	TorchVision [46]
	ResNeXt [79]	TorchVision [46]
	ViT-B/16 [18]	TorchVision [46]
	ViT-L/16 [18]	TorchVision [46]
	Swin-B/16 [41]	TorchVision [46]
	DeiT-B [64]	Timm [72]
	BEiT-B [4]	Timm [72]
	EfficientViT [6]	Timm [72]
	MLP-Mixer-B [63]	Timm [72]
	ConvMixer-B [65]	Timm [72]
Image Segmentation	Vision Mamba-B [89]	<a href="https://github.com/hustvl/Vim">https://github.com/hustvl/Vim</a>
	MambaVision-B [23]	<a href="https://github.com/NVlabs/MambaVision">https://github.com/NVlabs/MambaVision</a>
Object Detection	DeepLabV3+ [11]	<a href="https://github.com/VainF/DeepLabV3Plus-Pytorch">https://github.com/VainF/DeepLabV3Plus-Pytorch</a>
	SegFormer [78]	<a href="https://github.com/NVlabs/SegFormer">https://github.com/NVlabs/SegFormer</a>
Object Detection	Faster R-CNN [20]	<a href="https://github.com/facebookresearch/detectron2">https://github.com/facebookresearch/detectron2</a>
	DETR [8]	<a href="https://github.com/facebookresearch/detr">https://github.com/facebookresearch/detr</a>

## C.2 Implementation details

We train the perturbation generator for one epoch on the ImageNet-1K [55] dataset using the Adam [32] optimizer  $\beta = (0.5, 0.99)$ . We set the learning rate  $lr = 2e^{-4}$ .

Table S3: Training and evaluation dataset statistics.

Dataset	ImageNet-1K [55]	CUB-200-2011 [67]	Stanford Cars [33]	FGVC Aircraft [45]
Train	1.2 M	5,994 (Not Used)	8,144 (Not Used)	6,667 (Not Used)
Val.	50,000	5,794	8,041	3,333
# Classes	1,000	200	196	100
Resolution	224×224	448×448	448×448	448×448

**Dataset statistics.** We describe the statistics of the datasets used for training and evaluation in Table S3. Note that we do not use the training sets from CUB-200-2011 [67], Stanford Cars [33], or FGVC Aircraft [45] for the strict black-box cross-domain setting.

**Computational costs.** Since our approach only involves computational overheads during the training of the perturbation generator, there is *no inference time overhead*. During training, we describe in the table on the right that the time for a single forward pass with a batch size of 1 incurs an additional +12.18 (ms) relative to the baseline [86] time of 44.72 (ms), and an additional +28.31 (MB) in memory relative to the baseline memory requirement of 1,404.13 (MB), which are averaged over 1,000 iterations (See Table S4). We note that the training was performed on a single NVIDIA RTX A6000 GPU.

Table S4: Computational overheads with ours during training.

Training	Fwd time (ms)	Memory (MB)
Baseline [86]	44.72	1,404.13
w/ Ours	56.90 (+12.18)	1,432.44 (+28.31)

## C.3 Additional quantitative results

**Results with different surrogate models.** While we performed experiments against the VGG-16 surrogate model for fair comparison with previous works, we also provide, in Tables S5 and S6, our improvements when trained against other surrogate models such as VGG-19, ResNet-152, and DenseNet-169 as practiced in [86, 82, 83]. Ours added to the baseline trained against all three surrogate models across models and domains, except for cross-model against Dense169, consistently enhances the attack transferability. As with our results against VGG-16 in Tables 1 and 2, our method effectively boosts the attack capacity regardless of the type of surrogate model used for training the generator. We believe the slight increase in cross-model average when using DenseNet-169 as the surrogate model is driven mainly by pronounced gains on a few architectures (e.g. MNASNet and DeiT) while most other models also benefited, albeit to a lesser extent. In the cross-domain evaluation, adversarial examples generated with DenseNet-169 consistently deliver a substantial average performance boost, underscoring its effectiveness across differing data distributions.

In qualitative comparisons across different surrogate models in Fig. S4, our Grad-CAM [56] visualizations reveal activation patterns that depart significantly from the baseline. Rather than highlighting



only the main object region, our method further amplifies those top responses and draws out additional high-sensitivity areas that the baseline misses. When we step through the stages of adversarial noise generation, we see that our approach consistently places perturbations along object edges and contours. By focusing noise on these shared, model-agnostic features instead of scattering it elsewhere, our method not only seeks to align the generated adversarial noise with the most semantically meaningful regions but also achieves stronger transferability.

**Table S5: Additional quantitative cross-model transferability results.** We report the average improvement margins of our method added to the baseline [86] using different surrogate models (VGG-19, Res152, Dense169). We report the improvements ( $\Delta$  %) with ours relative to the baseline. Better averaged results are marked in **boldface**.

Cross-model		CNN										Transformer										Mixer		Mamba		Avg.
Method	Metric	Res50	Res152	Dense121	Dense169	IncV3	RegNetY	Mnas	SqueezeV2	EfficientV2	HRNet	ConvNeXt	ResNeXt	ViT-B	ViT-L	Swin-B	DeiT-B	BeiT-B	EfficientViT	MLP-B	Conv-B	Vim	Mamba	Vision		
Benign	Acc. (%)	74.60	77.33	74.22	75.74	76.19	77.95	66.50	61.96	67.91	63.65	82.12	76.64	77.24	77.56	79.78	82.27	83.95	69.97	72.26	78.04	77.89	82.72	74.28		
Surrogate model: VGG-19																										
BIA [86]	Acc. (%)	25.39	41.60	29.80	37.09	46.59	29.43	27.84	12.27	57.33	28.52	49.06	28.01	68.41	70.26	53.52	74.09	77.30	54.00	59.64	58.10	66.99	67.55	48.31		
	ASR (%)	67.84	48.70	62.10	53.52	42.23	64.15	60.65	80.07	30.66	58.18	42.21	65.27	14.73	12.84	35.33	12.43	10.62	26.91	24.60	28.64	17.17	20.95	39.88		
	FR (%)	72.08	58.40	67.47	59.46	49.46	68.23	67.51	84.49	37.52	65.50	47.07	69.74	22.49	20.48	41.64	18.59	15.20	37.27	33.93	35.79	24.84	26.46	9.04		
	ACR (%)	5.53	8.48	6.49	7.75	10.82	6.75	4.99	2.55	11.77	5.25	8.61	5.94	11.20	11.84	9.50	11.55	14.11	9.54	11.71	10.94	11.19	12.45	46.35		
BIA w/ ours	Acc. ( $\Delta$ %)	-1.49	+0.88	-1.70	-3.49	-4.04	-1.07	+1.06	-2.31	+0.46	-1.23	-4.40	+0.39	-0.24	-0.16	-6.38	-0.17	-0.32	+0.10	-0.55	-2.22	-2.29	-1.72	-1.40		
	ASR ( $\Delta$ %)	+1.93	-1.12	+2.17	+4.43	+5.18	+1.34	-1.43	+3.98	-0.65	+1.77	+5.18	-0.44	+0.35	+0.20	+7.63	+0.25	+0.32	-0.24	+0.75	+2.58	+2.75	+1.91	+1.77		
	FR ( $\Delta$ %)	+1.72	-0.89	+1.97	+3.95	+4.68	+1.24	-1.19	+2.89	-0.55	+1.42	+4.77	-0.37	+0.42	+0.15	+7.08	+0.09	+0.33	-0.33	+0.72	+2.48	+2.67	+1.95	+1.60		
	ACR ( $\Delta$ %)	-0.23	+0.11	-0.35	-0.56	-0.41	-0.13	+0.34	-0.18	-0.20	-0.29	-0.82	0.24	+0.14	-0.02	-1.45	+0.18	-0.33	-0.24	+0.06	-0.93	-0.68	-0.75	-0.30		
Surrogate model: Res152																										
BIA [86]	Acc. (%)	14.83	10.78	23.95	23.94	46.25	29.65	28.14	13.91	58.21	28.21	56.78	17.20	69.22	72.87	58.66	74.52	74.99	54.11	62.88	58.21	69.37	69.63	46.20		
	ASR (%)	81.29	86.82	69.55	70.18	42.50	63.77	60.43	77.30	29.43	58.60	33.27	78.79	13.71	9.85	29.18	11.90	13.51	26.43	20.51	28.56	14.15	18.42	42.64		
	FR (%)	83.73	88.41	73.91	74.15	49.64	67.83	67.60	82.80	36.33	65.83	30.73	81.35	21.64	17.34	35.99	18.01	18.47	36.49	29.89	35.39	21.75	23.91	48.60		
	ACR (%)	3.41	2.59	5.25	5.61	10.29	6.41	5.46	2.77	11.35	5.12	10.61	4.06	11.33	13.12	10.68	11.54	14.83	8.80	12.36	11.16	11.32	12.42	8.66		
BIA w/ ours	Acc. ( $\Delta$ %)	-0.61	-0.99	-2.96	-0.38	-5.13	-7.36	-5.35	-0.71	-3.87	-0.89	-6.17	-3.75	-0.12	-0.84	+0.67	-0.94	+0.20	+0.33	-2.37	-4.19	-9.23	-0.46	-2.51		
	ASR ( $\Delta$ %)	+0.78	+1.28	+3.76	+0.39	+6.36	+9.09	+7.37	+1.32	+4.75	+1.34	7.16	+4.70	+0.18	+1.13	-0.97	+0.92	-0.24	-0.32	+3.03	+5.09	+1.10	+0.48	+3.12		
	FR ( $\Delta$ %)	+0.78	+1.09	+3.23	+0.27	+5.70	+8.14	+6.29	+0.97	+4.37	+0.86	+6.79	+4.18	+0.17	+1.35	-1.04	+1.08	-0.28	-0.55	+2.96	+5.01	+10.83	+0.38	+2.84		
	ACR ( $\Delta$ %)	-0.10	+0.01	-0.69	-0.35	-1.21	-1.26	-1.33	+0.06	-0.50	-0.29	-1.56	-0.68	+0.07	+0.19	-0.50	-1.06	+0.02	+0.35	-0.37	-0.96	-2.64	-0.34	-0.60		
Surrogate model: Dense169																										
BIA [86]	Acc. (%)	6.96	13.84	6.60	6.45	38.57	6.96	13.84	6.60	6.45	14.58	24.22	13.53	65.52	71.19	32.44	59.37	64.44	42.66	49.89	36.04	38.97	61.97	30.96		
	ASR (%)	91.27	82.96	91.75	92.08	52.06	91.27	82.96	91.75	92.08	78.57	71.47	83.32	18.44	12.00	60.33	28.99	26.02	42.26	36.29	55.66	51.35	27.57	61.84		
	FR (%)	92.36	84.91	93.00	93.15	58.33	92.36	84.91	93.00	93.15	82.21	74.19	85.40	26.36	19.65	64.97	35.96	30.83	51.03	45.18	60.52	56.81	32.94	65.96		
	ACR (%)	1.77	2.91	1.85	1.85	8.59	1.77	2.91	1.85	1.85	2.58	4.19	3.19	11.09	13.07	3.87	5.37	14.58	7.51	7.84	6.54	4.86	11.91	5.54		
BIA w/ ours	Acc. ( $\Delta$ %)	-2.25	-7.65	-2.24	-2.76	-12.99	+4.65	+10.36	+2.34	+31.22	-6.50	+1.19	-6.71	-0.62	-0.73	+11.05	+8.35	+0.38	+0.58	+3.63	-2.67	+11.51	-7.61	+1.48		
	ASR ( $\Delta$ %)	+2.77	+9.41	+2.77	+3.38	+16.23	-5.34	-16.99	-6.14	-37.55	+9.68	-1.55	+8.22	+0.64	+0.70	-13.29	-9.27	-0.70	-0.77	-4.34	+3.20	-14.21	+8.67	-2.02		
	FR ( $\Delta$ %)	+2.41	+8.48	+2.32	+2.88	+13.97	-4.84	-12.84	-4.23	-33.64	+7.93	-1.23	+7.24	+0.76	+0.75	-12.09	-9.48	-0.70	-0.65	-4.29	+2.99	-12.99	+8.44	-1.76		
	ACR ( $\Delta$ %)	-0.73	-1.65	-0.71	-0.83	-2.64	+1.17	+1.78	+0.18	+6.26	-0.93	-0.40	-1.75	-0.54	-0.80	+2.23	+4.10	-1.31	+0.16	+1.46	-0.80	+2.00	-2.56	+0.17		

**Table S6: Additional quantitative cross-domain transferability results.** We report the average improvement margins of our method added to each baseline, averaged over three models for each domain using different surrogate models (VGG-19, Res152, Dense169). We report the improvements ( $\Delta$  %) with ours relative to the baseline [86]. Better averaged results are marked in **boldface**.

Cross-domain	CUB-200-2011 [67]				Stanford Cars [33]				FGVC Aircraft [45]				Avg.
Method	Acc ↓	ASR ↑	FR ↑	ACR ↓	Acc ↓	ASR ↑	FR ↑	ACR ↓	Acc ↓	ASR ↑	FR ↑	ACR ↓	Acc. (%)
Benign	86.91	N/A	N/A	N/A	93.56	N/A	N/A	N/A	92.07	N/A	N/A	N/A	90.85
Surrogate model: VGG19													
BIA [86] (%)	52.47	41.08	45.63	9.77	71.09	25.16	27.32	17.15	52.28	44.14	46.96	11.03	58.61
w/ Ours (Δ%p)	-10.05	+11.20	+10.39	-2.26	-11.48	+12.04	+11.73	-2.91	-10.87	+11.56	+11.04	-2.79	<b>-10.80</b>
Surrogate model: Res152													
BIA [86] (%)	49.52	44.51	48.53	9.96	50.71	46.60	48.44	12.81	40.43	56.83	59.14	9.01	46.89
w/ Ours (Δ%p)	-6.27	+7.07	+6.62	-0.82	+0.09	-0.15	-0.20	-0.43	-7.17	+7.72	+7.07	-0.87	<b>-4.45</b>
Surrogate model: Dense169													
BIA [86] (%)	30.01	66.46	68.97	6.73	34.08	64.13	65.34	9.29	23.23	75.24	5.74	76.44	29.11
w/ Ours (Δ%p)	-3.68	+4.04	+3.92	-1.20	-8.54	+8.99	+8.66	-2.32	-11.60	+12.32	+11.62	-3.36	<b>-7.94</b>

**Cross-task evaluations.** Cross-task results in Table S7 show only minor differences among existing generative attack methods, with all approaches achieving similarly low attack success rates in this setting. These uniformly modest outcomes highlight the difficulty of transferring adversarial examples crafted on an image classification-oriented surrogate model to tasks with different objectives, since the perturbations fail to align with the target task’s feature representations. Nevertheless, integrating our early-block semantic consistency into each baseline yields small but consistent improvements, demonstrating that preserving coarse semantic cues still provides a performance boost even under the strict black-box evaluation.

**Table S7: Comparison of cross-task attack strength with ours added to each baseline.** Ours further enhances the transferability consistently across semantic segmentation and object detection tasks. Boldface means better results.

Cross-task	Task					
	Semantic Segmentation (mIoU $\downarrow$ )			Object Detection (mAP50 $\downarrow$ )		
	DeepLabV3+ [11]	SegFormer [78]	Avg.	Faster R-CNN [20]	DETR [8]	Avg.
Benign	76.21	71.89	74.05	61.01	62.36	61.69
CDA [50]	25.63	<b>20.16</b>	22.90	32.78	26.29	29.54
w/ Ours	<b>25.16</b>	20.26	<b>22.71</b>	<b>31.98</b>	<b>25.68</b>	<b>28.83</b>
LTP [29]	23.71	26.97	25.34	29.39	22.41	25.90
w/ Ours	<b>22.27</b>	<b>26.68</b>	<b>24.48</b>	<b>26.85</b>	<b>22.18</b>	<b>24.52</b>
BIA [86]	23.89	25.60	24.75	28.43	21.01	24.72
w/ Ours	<b>22.05</b>	<b>24.75</b>	<b>23.40</b>	<b>28.34</b>	<b>20.70</b>	<b>24.52</b>
GAMA [1]	24.10	27.53	25.82	28.01	<b>20.71</b>	24.36
w/ Ours	<b>23.67</b>	<b>25.59</b>	<b>24.63</b>	<b>27.60</b>	<b>20.79</b>	<b>24.20</b>
FAEL [82]	23.75	26.40	25.08	27.94	20.91	24.43
w/ Ours	<b>23.38</b>	<b>25.01</b>	<b>24.20</b>	<b>27.64</b>	<b>20.29</b>	<b>23.97</b>
PDCL [83]	24.42	26.05	25.24	28.48	21.38	24.93
w/ Ours	<b>22.51</b>	<b>25.88</b>	<b>24.20</b>	<b>27.66</b>	<b>20.73</b>	<b>24.20</b>

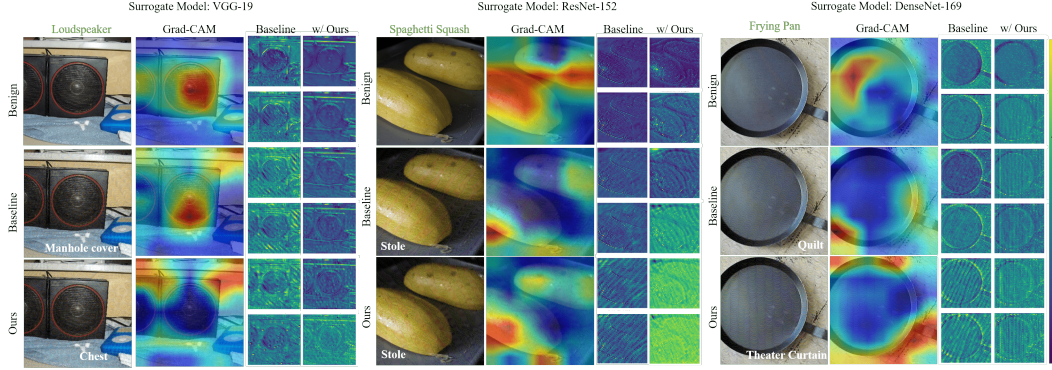


Figure S4: Comparison of the crafted AEs, Grad-CAMs, intermediate feature activation maps from the baseline, and with ours (columns 1–4, respectively). We present the qualitative results from training against other surrogate models: VGG-19 (Left), ResNet-152 (Center), and DenseNet-169 (Right) as commonly compared in existing generative attacks [86, 1, 82, 83]. The correct label and attacked prediction results are marked in **green** and white, respectively.

**Mid-level layer variations.** To further verify that our proposed method is compatible with the baseline [86] shown to perform best at the selected mid-level layer of the VGG-16 surrogate model (*i.e.*, Maxpooling.3), we conducted an ablation study on the mid-level layer in Fig. S5. Across domain, model, and two tasks (SS and OD), we observe that our method added to the baseline still maintains the best strength of the attack at the selected mid-level layer, Maxpooling.3, compared to the other early or late layers.

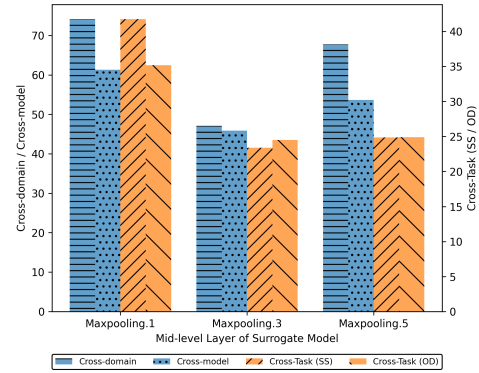


Figure S5: Ablation study on the mid-level layer of the VGG-16 surrogate model.

**Slight improvements in perceptual quality.** In Table 4, we compare PSNR, SSIM, and LPIPS scores for each baseline alone versus the same baseline augmented with our early-block semantic consistency mechanism. Across all baselines, adding our method results in a slight PSNR increase while SSIM and LPIPS remain effectively unchanged. These minimal or positive changes confirm that our approach does not introduce any perceptual degradation. Instead, it preserves, and in some cases slightly enhances, the visual fidelity of adversarial examples even as it strengthens their transferability.

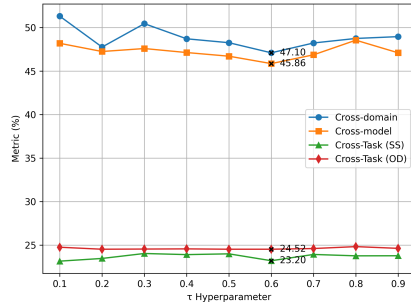


Figure S6: Sensitivity of  $\tau$  hyper-parameter.

**Ablation study on the hyperparameter  $\tau$ .** To assess the sensitivity of  $\tau$  in Eq. 2, we conducted a sweep of hyperparameter values in Fig. S6. Across the range of values from 0 to 1, we find that our optimal value of  $\tau = 0.6$  best balances the strength of the attack across all four cross-settings.

#### C.4 Additional qualitative results

In these additional qualitative results in Fig. S7, we observe two clear patterns in the adversarial masks. First, straight lines trace the edges of objects, reinforcing the primary structural cues. Second, circular ring shapes appear in the background, helping to disperse noise across non-object regions. Grad-CAM visualizations on the right show that our method also drives adversarial activations to much higher levels than those seen in the benign image and boosts areas that exhibited only modest responses under baseline attacks. By combining precise noise along the boundaries with amplified feature activations, our approach an-

chors noise to the most meaningful contours while strengthening weaker signals, producing stronger and more transferable adversarial examples.

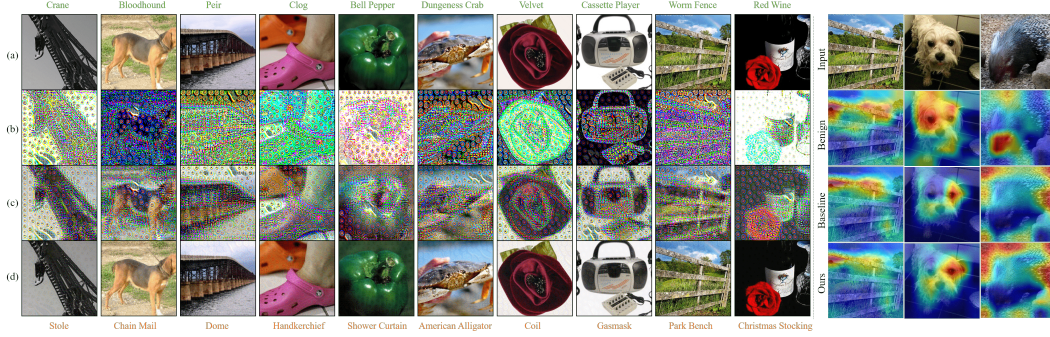


Figure S7: **Additional qualitative results.** Our semantic structure-aware attack successfully guides the generator to focus perturbations particularly on the semantically salient regions, effectively fooling the victim classifier. *Left:* (a) benign input image, (b) generated perturbation (normalized for visual purposes only), (c) unbounded adversarial image, and (d) bounded adversarial image. The label on top (green) and bottom (orange) denote the correct label and prediction after the attack, respectively. *Right:* We highlight that our method induces Grad-CAM [56] to focus on *drastically different regions* in our adversarial examples compared to both the benign image and the adversarial examples crafted by the baseline [86]. Moreover, our approach *noticeably spreads and reduces the high activation regions* observed in the benign and baseline cases, enhancing the transferability of our adversarial perturbations.

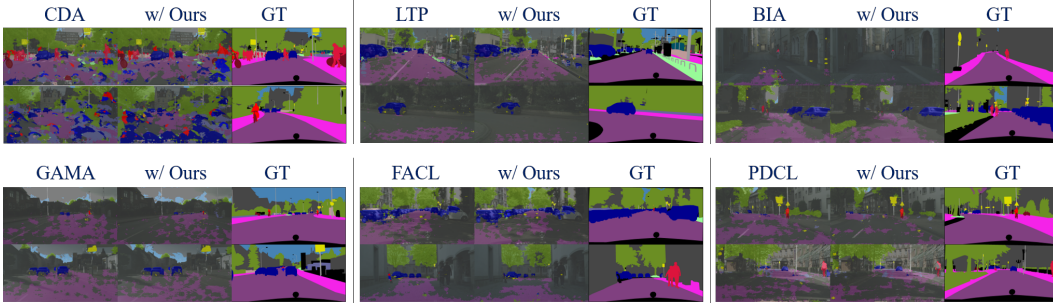


Figure S8: **Additional cross-task (SS) qualitative results.**

We also provide additional qualitative results on the cross-task (SS and OD) settings. In our additional segmentation examples in Fig. S8, we observe that our method does not just blur or hide parts of the road, but it actually makes the model stop recognizing entire road areas and even small objects like pedestrians or cars. The baseline attack might only erase a few isolated pixels or blend edges, but ours turns whole stretches of road into “ignore,” wiping out those predictions in one go. In other words, our method uniformly removes both large surfaces and tiny details, so the segmented map ends up missing key pieces of the scene that the baseline leaves untouched. Similarly, in our additional object detection examples in Fig. S9, our attack causes the model to stop predicting any localized boxes around objects (RoI), completely removing every predicted region of interest, whereas the baseline often leaves boxes in place or only shifts them slightly.

**Difference map analysis.** Following BIA [86] but expanding to all generator layers, we visualize the difference map in the feature activations between each baseline and ours added to it to better demonstrate the distinct noise our method further adds for enhanced transferability. To compute the difference map at each block, we take the activation map and apply cross-channel average pooling. Then, to better qualitatively highlight the added noise, we further threshold the difference map as follows:

$$\text{Diff}(\mathbf{g}_{\text{baseline}}^l, \mathbf{g}_{\text{ours}}^l) = \begin{cases} 1, & \mathbf{g}_{\text{ours}}^{l, \text{pooled}} - \mathbf{g}_{\text{baseline}}^{l, \text{pooled}} > 0, \\ 0, & \text{else,} \end{cases}$$



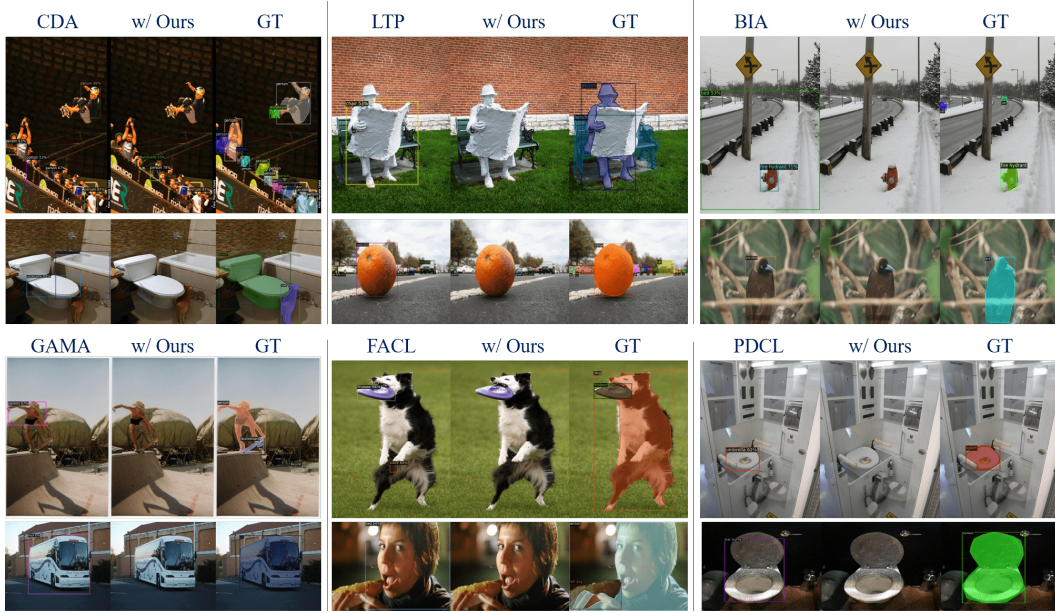


Figure S9: **Additional cross-task (OD) qualitative results.**

with  $\mathbf{g}_{\text{baseline}}^{l,\text{pooled}}$  and  $\mathbf{g}_{\text{ours}}^{l,\text{pooled}}$  defined as channel-wise averages as follows:

$$\mathbf{g}_{\text{baseline}}^{l,\text{pooled}} = \frac{1}{C} \left| \sum_C G_{\theta_{\text{baseline}}}^l(\mathbf{x}) \right|, \quad \mathbf{g}_{\text{ours}}^{l,\text{pooled}} = \frac{1}{C} \left| \sum_C G_{\theta_{\text{ours}}}^l(\mathbf{x}) \right|,$$

where  $G_{\theta_{\text{baseline}}}^l(\cdot)$  and  $G_{\theta_{\text{ours}}}^l(\cdot)$  denote  $l$ -th block activation map of the baseline and ours, respectively. In Fig. S10, we visualize the thresholded difference map mask in row 1, and the naïve difference map in row 2. We remark that, specifically in resblocks upon where we focus our method, adversarial noise generation is accentuated more along the object-salient regions, which are extracted by the preceding downsampling layers. Compared to each baseline, our method is observed to stress more on the semantic structure of the object in the image during adversarial noise generation, which primarily occurs in the intermediate residual blocks.

**Attack robustness against purification defense.** Further looking into how robust our attack performs against purification methods such as NRP [49], we report the improvements with Ours in Table S8. On most of the baselines, our method addition maintains lower Accuracy, ASR and FR scores than the baseline alone, while on the recent advanced methods (*e.g.* FACL [82] and PDCL [83]), our method very slightly maintains similar scores with those of the baseline alone on the three metrics. On the other hand, on the more challenging ACR metric, we observe that our method slightly improves from the baseline, entailing that our generative feature-level tuning further reduces the number of inadvertently corrected samples.

**Attack robustness on zero-shot image classification.** We also evaluated our method on the zero-shot image classification task with the well-known CLIP [52] vision-language model in Table ???. Here, we observe that, except for BIA [86] and FACL [82], we observe boosted attacked accuracy when we add our method to the baselines [50, 29, 1, 83]. We conjecture that the slight attack strength degradation owes to the baseline method that has already been well-fitted to generate adversarial examples effective for the zero-shot setting based on the relatively lower accuracy scores than the rest. We posit that the respective well-trained generator is already adept enough that our method may interfere with the learned generator weights negatively, and there may exist a maximum capacity at which AEs from generative model-based attacks can attack victim models.

**Random trials for Baseline [86] with Ours.** In Table S9, we further show that our method exhibits stable training results (mean $\pm$ std.dev.) as shown from multiple random seed trials evaluated on all four cross-settings.

Table S8: Adversarial transferability results with our method against purification method tested on Inc-V3 victim model, and random seed testing. Better results in **boldface**.

Method	Metric	Purification		Avg.
		NRP [49]	NRP-ResNet [49]	
Benign	Acc. %		76.19	
CDA [50]	Acc. (%) ↓	71.14	67.04	69.09
	ASR (%) ↑	10.29	15.94	13.11
	FR (%) ↑	17.45	24.00	20.73
	ACR (%) ↓	11.73	12.53	<b>12.13</b>
w/ Ours	Acc. (%) ↓	70.90	66.16	<b>68.53</b>
	ASR (%) ↑	10.73	17.07	<b>13.90</b>
	FR (%) ↑	18.15	25.25	<b>21.70</b>
	ACR (%) ↓	12.11	12.51	12.31
LTP [29]	Acc. (%) ↓	72.19	67.65	69.92
	ASR (%) ↑	8.82	15.22	12.02
	FR (%) ↑	15.59	23.15	19.37
	ACR (%) ↓	11.42	12.83	<b>12.13</b>
w/ Ours	Acc. (%) ↓	71.78	65.51	<b>68.65</b>
	ASR (%) ↑	9.45	17.97	<b>13.71</b>
	FR (%) ↑	16.34	25.98	<b>21.16</b>
	ACR (%) ↓	11.69	12.63	12.16
BIA [86]	Acc. (%) ↓	73.84	71.93	72.89
	ASR (%) ↑	6.37	9.20	7.79
	FR (%) ↑	12.46	16.35	14.41
	ACR (%) ↓	19.51	11.53	<b>11.02</b>
w/ Ours	Acc. (%) ↓	73.85	71.40	<b>72.63</b>
	ASR (%) ↑	6.36	10.00	<b>8.18</b>
	FR (%) ↑	12.63	17.31	<b>14.97</b>
	ACR (%) ↓	10.52	11.89	11.21
GAMA [1]	Acc. (%) ↓	74.42	72.30	73.36
	ASR (%) ↑	5.35	8.53	6.94
	FR (%) ↑	10.96	15.35	13.16
	ACR (%) ↓	9.67	10.96	<b>10.32</b>
w/ Ours	Acc. (%) ↓	74.31	71.78	<b>73.05</b>
	ASR (%) ↑	5.65	9.32	<b>7.49</b>
	FR (%) ↑	11.60	16.32	<b>13.96</b>
	ACR (%) ↓	10.17	11.29	10.73
FACL [82]	Acc. (%) ↓	74.23	71.95	<b>73.09</b>
	ASR (%) ↑	5.68	9.07	<b>7.38</b>
	FR (%) ↑	11.57	15.94	<b>13.76</b>
	ACR (%) ↓	9.94	11.22	10.58
w/ Ours	Acc. (%) ↓	74.21	72.00	73.11
	ASR (%) ↑	5.69	8.98	7.34
	FR (%) ↑	11.42	15.81	13.62
	ACR (%) ↓	9.90	11.11	<b>10.51</b>
PDCL [83]	Acc. (%) ↓	74.04	71.55	<b>72.80</b>
	ASR (%) ↑	6.16	9.63	<b>7.90</b>
	FR (%) ↑	12.26	16.82	<b>14.54</b>
	ACR (%) ↓	10.66	11.34	11.00
w/ Ours	Acc. (%) ↓	74.17	71.76	72.97
	ASR (%) ↑	5.92	9.32	7.62
	FR (%) ↑	11.91	16.43	14.17
	ACR (%) ↓	10.45	11.20	<b>10.83</b>

Table S9: Attack robustness on zero-shot image classification task with CLIP [52].

	CLIP	ViT-B/16 (%)	Acc. (Δ%p)	ViT-B/32 (%)	Acc. (Δ%p)
Benign		66.10	-	61.02	-
CDA [50]		40.34	-	32.53	-
w/ ours		40.22	<b>-0.12</b>	32.07	<b>-0.46</b>
LTP [29]		40.61	-	33.36	-
w/ ours		40.21	<b>-0.40</b>	33.20	<b>-0.16</b>
BIA [86]		39.27	-	32.16	-
w/ ours		39.78	+0.51	32.70	+0.54
GAMA [1]		40.10	-	33.18	-
w/ ours		39.87	<b>-0.23</b>	32.98	<b>-0.20</b>
FACL [82]		39.50	-	32.69	-
w/ ours		39.63	+0.13	32.92	+0.23
PDCL [83]		40.16	-	33.11	-
w/ ours		39.58	<b>-0.58</b>	32.76	<b>-0.35</b>

Table S10: Random trials for Ours added to the baseline [86].

Trial	Cross-	Accuracy (↓)	ASR (↑)	FR (↑)	ACR (↓)
1	Domain	47.99	48.14	50.81	10.24
	Model	46.12	42.67	48.69	8.34
	Task (OD)	24.51 (mAP50)			
	Task (SS)	23.02 (mIoU)			
2	Domain	47.95	48.19	50.86	10.31
	Model	46.26	42.53	48.49	8.32
	Task (OD)	24.52 (mAP50)			
	Task (SS)	24.33 (mIoU)			
3	Domain	47.10	49.02	51.66	9.66
	Model	45.86	43.04	49.00	8.28
	Task (OD)	24.52 (mAP50)			
	Task (SS)	23.20 (mIoU)			
Avg.	Domain	47.58 ± 0.41	48.45 ± 0.40	51.11 ± 0.39	10.07 ± 0.29
	Model	46.08 ± 0.17	42.75 ± 0.22	48.73 ± 0.21	8.31 ± 0.03
	Task (OD)	24.52 ± 0.01 (mAP50)			
	Task (SS)	23.52 ± 0.58 (mIoU)			

**Limitations and Societal Impacts.** Our method exposes vulnerabilities in generative attack pipelines, yet its transferability gains remain bounded by the underlying generator architecture. If early-intermediate block features lack rich semantic cues, or if a generator is designed to learn per-layer semantics differently (*e.g.* U-Net), our distillation mechanism to preserve the semantic integrity of the input yields only limited improvements. Although we demonstrate limited transferability on tasks beyond image classification (*e.g.* object detection and segmentation) in a scoped set of experiments, broader evaluation across additional tasks and domains remains necessary. By revealing these constraints in publicly available generative models, we contribute to neural network safety. The demonstrated transferability of semantic-aware perturbations underscores the need for adversarial robustness and motivates integrating safety measures, such as early-block regularization or semantic-consistency checks, into future network designs. Moreover, our approach targeting the adversarial perturbation process directly differs in principle from those that explicitly target benign-adversarial divergence. Therefore, our method stands as a compatible method to further enhance those methods, not to be assessed on the same grounds.



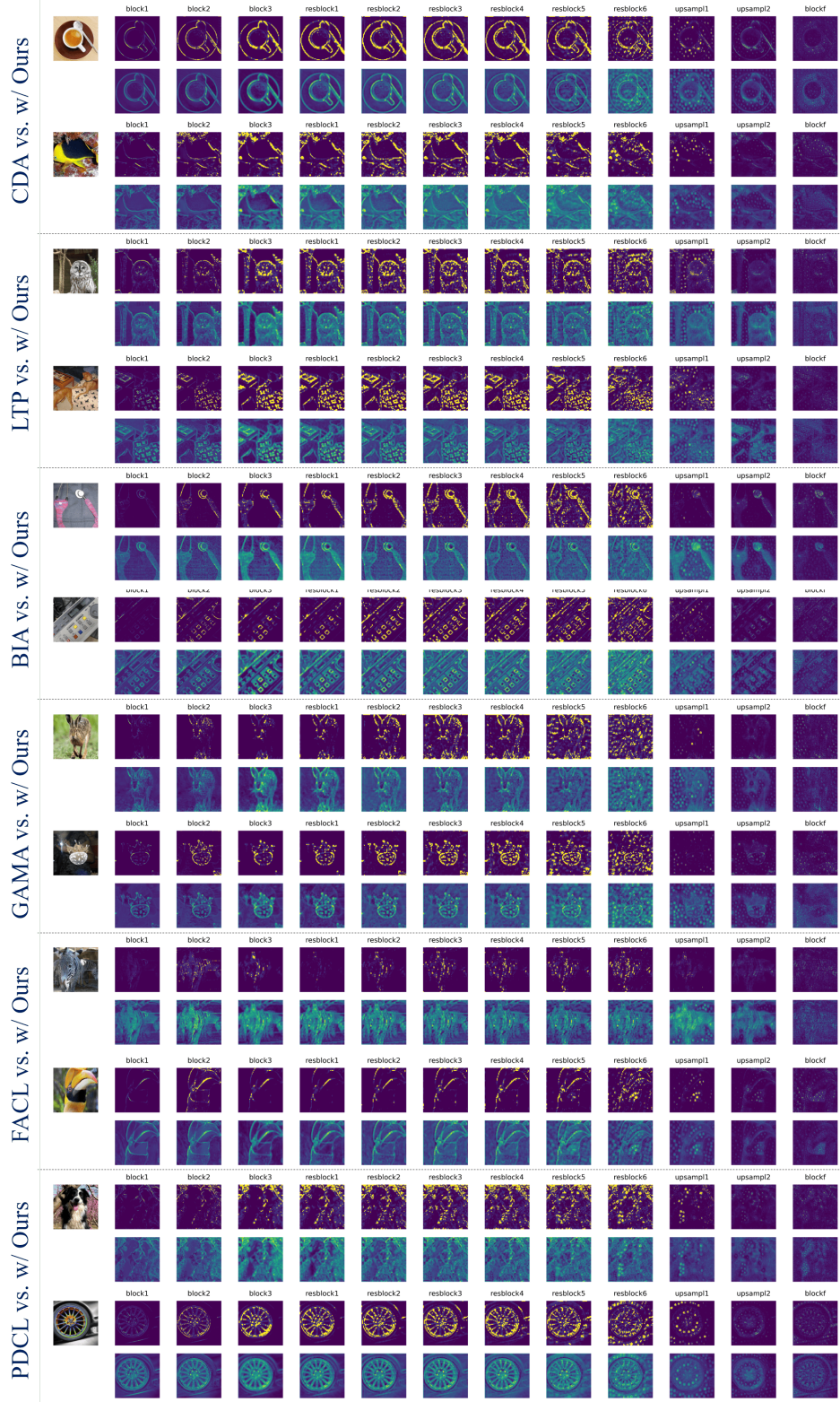


Figure S10: **Difference map comparisons.** Our method adds noticeable object-salient noise to the intermediate block features in the generator, as visible by the distinctive difference from each baseline. For each input on the leftmost column, we visualize the output feature map of each block in the generator in each column (*left*→*right*): thresholded binary mask (*top*) and feature activation difference maps (*bottom*). In the in the *resblocks* in particular, our method further adds noticeable adversarial noise centered around the object’s semantic structure relative to each baseline, demonstrating the enhanced noise generation progression with our approach.